Atmospheric Research 246 (2020) 105122

Contents lists available at ScienceDirect

Atmospheric Research

journal homepage: www.elsevier.com/locate/atmosres

Evaluation of CMIP5 models and projected changes in temperatures over South Asia under global warming of 1.5 °C, 2 °C, and 3 °C

Safi Ullah[a], Qinglong You[b,a,*], Yuqing Zhang[b], Asher Samuel Bhatti[c], Waheed Ullah[c], Daniel Fiifi Tawia Hagan[c], Amjad Ali[d], Gohar Ali[e,f], Mushtaq Ahmad Jan[d], Shah Nawaz Khan[d], Asif Ali[g]

[a] Key Laboratory of Meteorological Disaster, Ministry of Education (KLME), Joint International Research Laboratory of Climate and Environmental Change (ILCEC), Collaborative Innovation Center on Forecast and Evaluation of Meteorological Disasters (CIC–FEMD), Nanjing University of Information Science and Technology (NUIST), Nanjing 210044, China

[b] Department of Atmospheric and Oceanic Sciences, Institute of Atmospheric Sciences, Fudan University, Shanghai 200438, China

[c] Collaborative Innovation Center on Forecast and Evaluation of Meteorological Disasters (CIC–FEMD), School of Geographical Sciences, Nanjing University of Information Science and Technology (NUIST), Nanjing 210044, China

[d] Centre for Disaster Preparedness & Management, University of Peshawar, 25000 Peshawar, Pakistan

[e] School of Atmospheric physics, Nanjing University of Information Science & Technology (NUIST), Nanjing 210044, China

[f] Pakistan Meteorological Department, Sector H–8/2, 44000 Islamabad, Pakistan

[g] Department of Disaster Management, National University of Science and Technology (NUST), Islamabad 44000, Pakistan

ARTICLE INFO

Keywords:
CMIP5
South Asia
1.5 °C
2 °C
3 °C

ABSTRACT

This study was designed to evaluate the spatiotemporal performance of the Coupled Model Intercomparison Project Phase 5 (CMIP5) models in the historical simulation and future projections of minimum (T_{min}), maximum (T_{max}), and mean temperature (T_{mean}) over South Asia (SA) during global warming of 1.5 °C, 2 °C, and 3 °C targets under RCP4.5 and RCP8.5 scenarios. It is worth mentioning that the present study is the first of its kind to use such a large number of CMIP5 models to project future changes in T_{min}, T_{max}, and T_{mean} over SA using three different warming thresholds. The results show that CSIRO–MK3–6–0, MIROC–ESM–CHEM, CNRM–CM5, CCSM4, and MRI–CGCM3 models relatively performed better with a consistent and accurate spatiotemporal simulation of T_{min}, T_{max}, and T_{mean} over SA. In terms of projected changes, T_{min}, T_{max}, and T_{mean} show a dominating and consistent warming pattern over SA with stronger intensity in higher latitude than mid–low latitudes under 1.5 °C, 2 °C, and 3 °C warming thresholds. The northwestern (eastern) regions of SA will witness greater (least) warming in T_{min}, T_{max}, and T_{mean} under all warming thresholds in RCP4.5 and RCP8.5 scenarios. Furthermore, the central and southern parts of SA will experience a moderate increase in T_{min}, T_{max}, and T_{mean} under all warming targets. The uneven and intensified patterns of T_{min}, T_{max}, and T_{mean} may result in temperature extremes, which would pose potential risks to the local population. Therefore, more attention should be paid on the regional and local perspectives to estimate the adverse impacts of these extremes under different global warming targets. We further suggest to project future changes in climate extremes over SA under different warming levels, which will be helpful in climate change adaptation and mitigation over the study region.

1. Introduction

During the Paris Agreement of the United Nations Framework Convention on Climate Change (UNFCCC), it was proposed to "stabilize the global mean temperature to well below 2 °C and limit to 1.5 °C above the pre–industrial levels through sustained efforts" (UNFCCC, 2015). The ambitious target of stabilizing global warming to 1.5 °C above the pre–industrial levels would significantly reduce vulnerability to climate change, which could certainly help in achieving the goal of climate change adaptation and mitigation (Dosio et al., 2018; Ford et al., 2018; Li et al., 2018). Following the Paris Agreement, the Intergovernmental Panel on Climate Change (IPCC) issued a special

* Corresponding author at: Key Laboratory of Meteorological Disaster, Ministry of Education (KLME), Joint International Research Laboratory of Climate and Environmental Change (ILCEC), Collaborative Innovation Center on Forecast and Evaluation of Meteorological Disasters (CIC–FEMD), Nanjing University of Information Science and Technology (NUIST), Nanjing 210044, China.

E-mail address: yqingl@126.com (Q. You).

https://doi.org/10.1016/j.atmosres.2020.105122
Received 31 December 2019; Received in revised form 23 June 2020; Accepted 27 June 2020
Available online 04 July 2020
0169-8095/

report on the impacts of global warming under 1.5 °C and 2 °C targets, which indicated that a warming of 1.5 °C to 2 °C above the pre–industrial levels will increase the risk of climate extremes and would affect human life, water resources, food production, and ecosystems (IPCC, 2018). Though, the findings of recent studies revealed that the impacts of global warming under 1.5 °C and 2 °C targets will be disastrous (Donnelly et al., 2017; Liu et al., 2018; Nangombe et al., 2018), yet there is a lack of quantitative analysis and knowledge on the benefits of limiting global warming to such a level (Jacob et al., 2018; Lee and Min, 2018; Lehner et al., 2017). In this regards, the efforts of the scientific community still continue to provide an integrated and consolidated basis for assessment of climate change and its impacts under different warming levels at global and regional scales.

In recent years, the concept of climate change projections under different global warming targets gained great attention from the scientific community. So far, many studies have been conducted to understand and quantify the impacts of +1.5 °C warming at global and regional scales. Recently, Dosio et al. (2018); Liu et al. (2018) assessed changes in 1.5 °C and 2 °C warming targets at the global scale. Similarly, Xu et al. (2017); Lee and Min (2018) estimated the impacts of 1.5 °C and 2 °C warming levels over Asia. A large number of studies have also been conducted to estimate the impacts of climate change over Africa during +1.5 °C warming levels (Nangombe et al., 2018; Sylla et al., 2018). Moreover, King et al. (2017) predicted that Australia will experience severe extreme events under +1.5 °C global warming. Several studies have projected long-lasting impacts of climate change over Europe during +1.5 °C warming world (Dosio and Fischer, 2018; Jacob et al., 2018). Similarly, Lehner et al. (2017); Colón-González et al. (2018) estimated the impacts of climate change over North and South America under global warming of +1.5 °C. Previously, most of these studies have overlooked the 3 °C warming target, though its adverse impacts are expected to be more severe and intense than the 1.5 °C and 2 °C warming targets.

South Asia (hereafter SA) is spread over eight countries including; Afghanistan, Bangladesh, Bhutan, India, Nepal, Maldives, Pakistan, and Sri Lanka (Naveendrakumar et al., 2019); however, this study focuses on the continental parts of SA, where previous literature has already reported an alarming increase in temperature than coastal regions and adjacent islands. Thus, we excluded the Sri Lankan and Maldives islands from the present study. SA is a home to more than 1.5 billion people, which is expected to be raised to 2 billion population by the mid-21st century (Jones and Neill, 2016; Xu et al., 2020). Under the recent global warming trends, the region is considered as one of the sharp rising temperature zones and major hotspot of climate change (Byers et al., 2018; Ullah et al., 2019b; Xu et al., 2020). Due to its distinct location, complex topography, and diverse climatology, this region is highly vulnerable to climate extremes. Moreover, high population density, rapid urbanization, high poverty ratio, and low adaptive capacity further exacerbate vulnerability of the region to climate change-induced extremes (Aadhar and Mishra, 2020; Im et al., 2017; Khan et al., 2018b). Although per capita GDP across SA has increased substantially in recent past, yet the fingerprints of real poverty and marginalization exist with much higher proportion, which would intensify the exposure of people to future climate extremes. As the economies of the SA countries rely much on agriculture, natural resources, forestry, and fisheries, the rising risk of floods, droughts, and heatwaves would decrease production of these sectors and aggravate the condition of the local poor people (Im et al., 2017; Wu et al., 2019; Yadav and Lal, 2018; Zhou et al., 2020).

In recent decades, SA has experienced several climate extremes such as heatwaves, floods, and droughts, which is expected to be continued in the future with more catastrophic impacts (Aadhar and Mishra, 2020; Naveendrakumar et al., 2019; Yadav and Lal, 2018). In 2015, the central parts of SA, i.e., western India and eastern Pakistan, experienced the deadly heatwaves in 2015, which resulted in more than 2,500 deaths in India and more than 1,200 deaths in Pakistan (Khan et al., 2018b; Ratnam et al., 2016; Ullah et al., 2019b; Wehner et al., 2016). During 2018 and 2019, Bangladesh witnessed the history worst floods, which claimed more than 119 human lives and affected 307,000 people with the destruction of 580,000 houses (Alam et al., 2020; Naveendrakumar et al., 2019; Rahman and Islam, 2019). Similarly, Pakistan faced a series of catastrophic floods in 2010, which inundated 78 districts with 20 million victims and 2000 deaths (ADB, 2010; Rahman and Khan, 2011). The study region also experienced a consistent dry and hot period during 1997-2002, which resulted in severe droughts over Pakistan and some parts of Afghanistan, India and Iran (Ahmed et al., 2016; Amirataee et al., 2018; Naveendrakumar et al., 2019; Shafiq and Kakar, 2007; Singh et al., 2019; Xie et al., 2013). This calamity has adversely affected the economy and human subsistence of the said countries with maximum destruction in Baluchistan and Sindh provinces of Pakistan.

Several studies projected that the region will experience severe and frequent climate extremes in the future due to sharp rise in temperature (Im et al., 2017; Khan et al., 2019; Nasim et al., 2018). Recently, Aadhar and Mishra (2019) reported that half of the SA will be under severe dryness by the end of 21st century, which will affect 790, 890, and 1960 million people under 1.5 °C, 2 °C, and 2.5 °C warming levels, respectively. In another study, Aadhar and Mishra (2020) projected that the major parts of SA are expected to experience an increase in drought frequency under 1.5 °C, 2 °C, and 2.5°C warming worlds. In a recent study, Xu et al. (2020) reported an increase of 78 days/year in the frequency of heat extremes over South Asia during 2046–2054 under RCP8.5 scenario. Im et al. (2017) reported that SA is likely to face deadly heatwaves in the future with maximum tendency over the densely populated agricultural regions of the Ganges and Indus river basins. According to Yaduvanshi et al. (2019), India is highly sensitive to future temperature as 35% of the country is projected to witness a temperature change equal to or less than global mean temperature of 1.5°C and 2.0°C, while 65% of the country is expected to experience a substantial rise in temperature with maximum intensity in the northwestern parts. According to Mishra et al. (2017), India is expected to experience a 30-times rise in heatwaves and 92-times increase in population exposure by the end of 21st century under 2 °C warming world with respect to the pre-industrial levels. It is also anticipated that Bangladesh will exhibit a warming trend in seasonal temperature and its extremes under 1.5 °C, 2 °C, and 4 °C warming levels (Khan et al., 2020a, 2020b). In addition, many studies projected an increase in the frequency, intensity, duration, and extent of future temperature extremes with substantial socioeconomic impacts over the southwestern and northwestern parts of SA (Khan et al., 2019; Mazdiyasni et al., 2017; Nasim et al., 2018; Saeed et al., 2017; Wu et al., 2019). Despite a critical indicator of climate change, the projection of future changes in temperature over SA received less attention, while considering different global warming targets. In this regard, the present study was designed to estimate future changes in temperature of SA in 1.5 °C, 2 °C, and 3 °C warming worlds relative to the pre–industrial level.

This study comprises of two main parts. The first part aims to evaluate the performance of the 21 CMIP5 models in the historical simulation of surface minimum, maximum, and mean temperature (hereafter T_{min}, T_{max}, and T_{mean}) over SA and rank these models according to their spatiotemporal performances. The second part attempts to project the future changes in T_{min}, T_{max}, and T_{mean} over SA based on the corresponding multi-model ensemble means (MMEMs) of 21 models under global warming of 1.5 °C, 2 °C, and 3 °C targets. To the best of our knowledge, this study is the first of its kind to use such a large number of CMIP5 models to project changes in T_{min}, T_{max}, and T_{mean} over SA using three different warming thresholds. This study will provide a basis for the projection of future climate extremes over SA under different global warming thresholds. Moreover, the findings of the study will provide potential socio–economic implications for policy–makers to design climate change adaptation and mitigation strategies in the region.

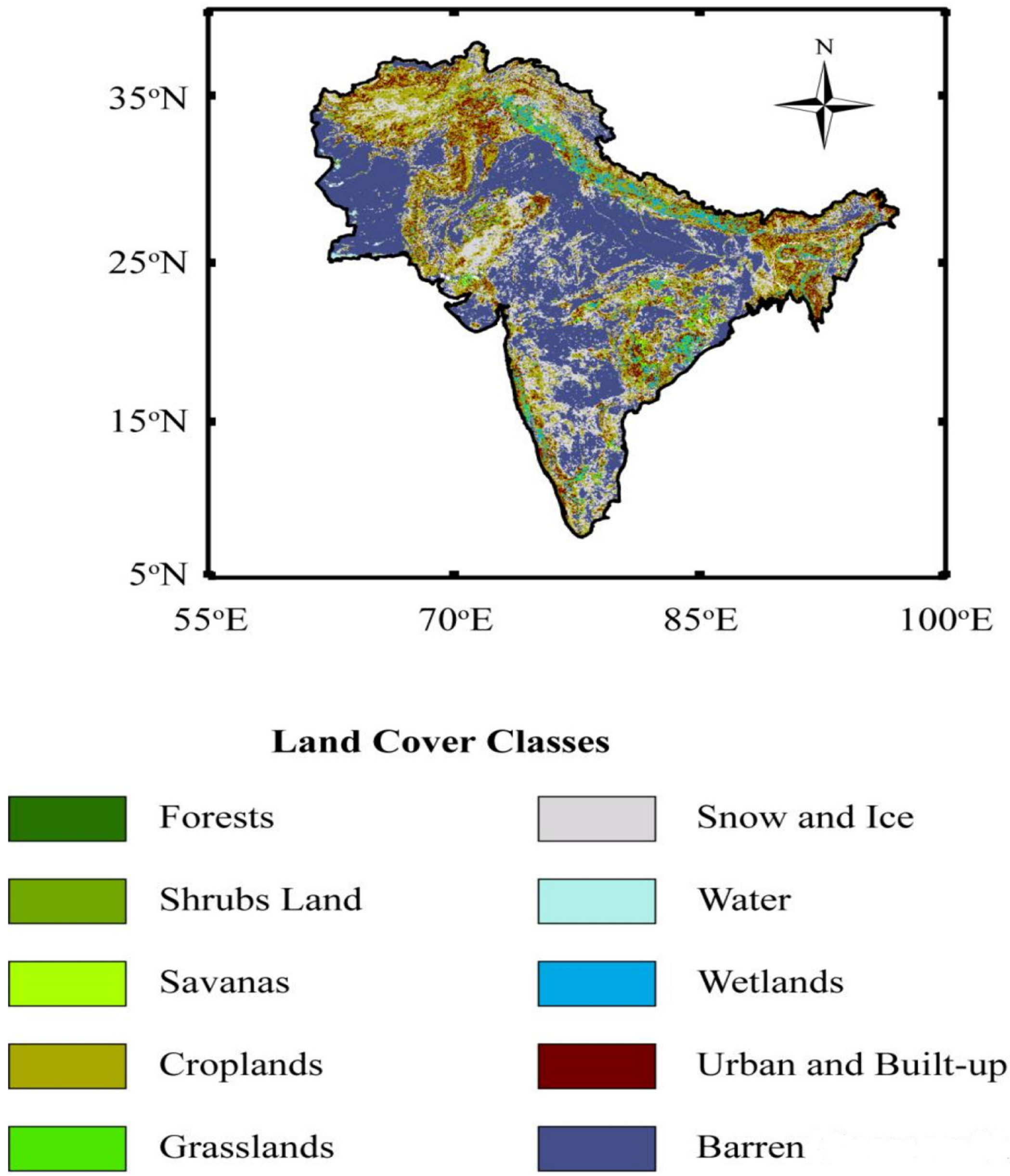

Fig. 1. Location map of the study area with land cover classes

2. Study area

SA is located in the southern part of the Asian continent between the 5°–35°N latitudes and 65°–95°E longitudes with 5,134,613 km^2 of landmass (Haq et al., 2017; Ramachandran and Kedia, 2013) (Fig. 1). The topography of the region is complex with world highest mountain range "Hindu Kush Himalayan (HKH) range" in the north, the Indian Ocean in the south, deserts, and plains in the central parts (Ren et al., 2017; Sun et al., 2017). The climate of SA varies from arctic temperature in the high mountainous regions to a temperate environment in the north to tropical conditions in the central–south (Haq et al., 2017; Ullah et al., 2018a). The variations in seasonal and annual temperature are highly influenced by diverse topography and geographical location of SA, which ultimately affects its overall climatology (Sun et al., 2017; Ullah et al., 2018b).

The SA annual water cycle is dependent on two dominant circulation systems that include the western disturbances and monsoon circulation system (Chen et al., 2019; Hunt et al., 2018; Li et al., 2017). All these together provide more than 80% of the annual precipitation budget to the study region (Aadhar and Mishra, 2020; Naveendrakumar et al., 2019). In addition, these weather systems have strong influences on regional temperature and its extremes both directly and indirectly (Galarneau et al., 2012; Hunt et al., 2018). The western disturbances are low-pressure systems that originate from the Mediterranean and contribute to the SA water cycle including; Afghanistan, Pakistan, India, and adjacent countries during winter season (Ahmed et al., 2018; Dimri et al., 2015; Filippi et al., 2014). These low-pressure systems indeed produce relatively less precipitation than monsoon system; however, their occurrence is greatly linked with the regional food security in the rainfed regions (Ahmed et al., 2019c; Yadav and Lal, 2018). The second and most dominant precipitation system is summer monsoon system, which is mostly active from June to September, and contributes more than 65% of the precipitation to the local water cycle (Joshi and Kar, 2018; Medina et al., 2010; Wang et al., 2017a). The SA monsoon is fed from multiple sources that include the Indian Ocean as a primary source of the water vapors, whereas the regional contributions also include as a fraction of water vapor from Ganges basin, Red sea and the neighboring Gulf region (Kripalani et al., 2007; Pathak et al., 2017a). Failure of any of these two-precipitation systems can affect the regional water supply in terms of heavy floods in Bangladesh, India, and Pakistan, landslides in the Himalayas, and severe droughts and crop failure in major river basins of the region (Ahmed et al., 2019c; Azad et al., 2013; Chen et al., 2019; Dimri et al., 2015; Gupta and Jain, 2018; Latif et al., 2017; Rasmussen et al., 2015; Wu et al., 2019).

3. Data and methods

3.1. Data

The observed monthly datasets of T_{min}, T_{max}, and T_{mean} over SA are obtained from the Climate Research Unit data (CRU TS 3.10) with a horizontal resolution of $0.5^{\circ} \times 0.5^{\circ}$ (Harris et al., 2014). Due to several advantages, we preferred the CRU data over other gridded products (Trenberth et al., 2014). The data have been developed from relatively a large number of in-situ data with a longer temporal scale (Ahmed et al., 2019c; Harris et al., 2014). In addition, a number of quality control procedures and approaches have been used during the development of CRU data, which have made the data more reliable and better than other gridded products (Kumar et al., 2007; Sun et al., 2018; Trenberth et al., 2014). Moreover, the thin plate smoothing splines interpolation technique has been employed to produce the CRU data, which is one of the robust techniques for interpolation (Ahmed et al., 2019b; New et al., 2002; Sun et al., 2014). Recently, several studies have reported better agreement of CRU data with the station record over different parts of SA (Adnan et al., 2015; Ahmed et al., 2019c; Asmat and Athar, 2017; Das et al., 2018; Kumar et al., 2007; Latif et al., 2018). The time period of all CRU datasets is from 1951 to 2005.

In addition, the monthly T_{min}, T_{max}, and T_{mean} outputs of 21 CMIP5 models are obtained from the CMIP5 data archive (http://cmip-pcmdi.llnl.gov/cmip5/index.html) (Taylor et al., 2012). The details of these models are provided in Table 1. The models' data include the historical (1861–2005) and the future (2006–2099) periods. The models are selected on the basis of their complete simulation data of two representative concentration pathway (RCP) scenarios, i.e., RCP4.5 and RCP8.5 for the period 2006–2099. The new emission scenarios of CMIP5 models are based on high–range (RCP8.5), mid–range (RCP4.5), and low–range emission scenarios (RCP2.6) (Wu et al., 2020; You et al., 2019). In this study, we used RCP8.5 and RCP4.5 scenarios to anticipate the largest possible changes in temperature, since these scenarios show the highest level of radiative forcing of up to 8.5 Wm^{-2} and 4.5 Wm^{-2} under given specific levels of greenhouse gas concentrations, respectively (Zhang et al., 2018). To facilitate analysis and get a common spatial resolution, a bilinear interpolation scheme was employed to regrid all model outputs to the same resolution as that of the observed data ($0.5^{o} \times 0.5^{o}$ grid) (Das et al., 2018; Seong et al., 2017).

3.2. Models evaluation

In the first part, the monthly T_{min}, T_{max}, and T_{mean} simulations and observations covering 1951–2005 are analyzed in order to evaluate the performance of CMIP5 models and ranked them accordingly. The Taylor diagram is used to evaluate the spatial skill of the models, which concisely quantify the degree of correspondence between simulated and observed datasets in their spatial patterns (Taylor, 2001). This technique consists of the three error metrics, which are interdependent and provide a statistical summary of comparisons between two spatial patterns: the correlation coefficient (*R*), the ratio of standard deviation (*Std*), and the unbiased root mean–square difference (*ub*RMSD) (Miao et al., 2014; Zhang et al., 2017). The *R* measures the degree of similarity within the temporal variabilities of two fields, while the *ub*RMSD expresses the differences within the datasets without the impact of the biases that may exist within the mean and amplitude of the datasets (Hagan et al., 2019; Wang et al., 2018). Similarly, the *Std* would rather quantify the ratio of the amplitudes of the two fields (Ullah et al., 2019; Wang et al., 2016). In this study, the model simulation results are best when the *R* and *Std* values are equal to 1 and *ub*RMSD value is close to 0 (Jiang et al., 2015).

Several studies stated that CMIP5 models generally do not produce accurate results in terms of interannual variations of climate variables (Jiang et al., 2015; You et al., 2018); therefore, we employed the interannual standard deviation as an Interannual Variability Skill (IVS) to explore the temporal skill of models relative to observed data (Zhang et al., 2017). The IVS is calculated as follows:

$$\mathrm{IVS} = \left(\frac{Std_m}{Std_o} - \frac{Std_o}{Std_m}\right)^2 \tag{1}$$

where Std_m and Std_o represent the interannual standard deviation of simulations and observations, respectively. Theoretically, an IVS value close to zero is a simulation that exactly corresponds to the observation.

To assess the overall model's ability to simultaneously simulate

Table 1
Details of the selected CMIP5 models (i.e., model name, originating group/country, and atmospheric resolution)

Model name	Modeling center (or group)	Atmospheric resolution (Lon × Lat)
ACCESS1–0	Commonwealth Scientific and Industrial Research Organization and Bureau of Meteorology, Australia	1.875° × 1.25°
BCC–CSM 1–1	Beijing Climate Center, China Meteorological Administration, China	2.8125° × 2.8125°
BNU–ESM	College of Global Change and Earth System Science, Beijing Normal University, China	2.8125° × 2.8125°
CanESM2	Canadian Centre for Climate Modelling and Analysis, Canada	2.8125° × 2.8125°
CCSM4	National Center for Atmospheric Research, USA	1.875° × 0.625°
CESM1–BGC	Community Earth System Model Contributors, USA	1.875° × 0.625°
CNRM–CM5	Centre National de Recherches Météorologiques / Centre Européen de Recherche et Formation Avancéeen Calcul Scientifique, France	1.4118° × 1.4063°
CSIRO–MK3–6–0	Commonwealth Scientific and Industrial Research Organization/Queensland Climate Change Centre of Excellence, Australia	1.875° × 1.875°
GFDL–CM3	Geophysical Fluid Dynamics Laboratory, USA	2.5° × 2°
GFDL–ESM2G		2.5° × 2°
GFDL–ESM2M		2.5° × 2°
INMCM4	Institute for Numerical Mathematics, Russia	2° × 2.5°
IPSL–CM5A–LR	Institut Pierre–Simon Laplace, France	3.75° × 1.875°
IPSL–CM5A–MR		2.5° × 1.2587°
MIROC5	The University of Tokyo, National Institute for Environmental Studies, and Japan Agency for Marine–Earth Science	1.4063° × 1.4063°
MIROC–ESM–CHEM	and Technology, Japan	2.8125° × 2.8125°
MIROC–ESM		2.8125° × 2.8125°
MPI–ESM–LR	Max Planck Institute for Meteorology, Germany	1.875° × 1.875°
MPI–ESM–MR		1.875° × 1.875°
MRI–CGCM3	Meteorological Research Institute, Japan	1.125° × 1.125°
NorESM1–M	Norwegian Climate Centre, Norway	2.5° × 1.875°

T_{min}, T_{max} and T_{mean}, we measured the rank of T_{min}, T_{max}, and T_{mean} based on the relevant Taylor diagram and IVS scores (You et al., 2018; Zhang et al., 2017). The overall ranking of each model has considered both spatial and temporal skills of the models in simulating T_{min}, T_{max}, and T_{mean}. The comprehensive rating index (CRI) is employed to effectively rank models (Jiang et al., 2015). The equation is as follows:

$$\mathrm{CRI} = 1 - \frac{1}{\mathrm{m} \times \mathrm{n}} \sum_{i=0}^{n} \mathrm{rank}_i \quad (2)$$

where m and n are the number of models (21) and variables, respectively. The CRI close to 1 indicates better model performance.

3.3. Temperature Projection

In the second part, we used MMEMs of 21 CMIP5 models to project future changes in T_{min}, T_{max} and T_{mean} under global warming of 1.5 °C, 2 °C, and 3 °C. The use of MMEM is a robust method to decrease uncertainties in the projection of future climate (Moss et al., 2010; Sylla et al., 2018), as it contains information from all contributing models and is more effective than a single model output (Guo et al., 2017; Miao et al., 2014). For the projection of future changes, we used the future period of 2006–2099 under two RCP scenarios (RCP4.5 and RCP8.5). The global warming targets used in this study are relative to the pre–industrial levels (1861–1880), and serve to define years in which global warming would reach or exceed the 1.5 °C, 2 °C, and 3 °C levels under the RCP4.5 and RCP8.5 scenarios (Jacob et al., 2018; Liu et al., 2018). Here, we calculated the regional mean surface temperature anomaly for 30–year running mean based on MMEMs of the selected models above the pre–industrial levels. In order to obtain 1.5°C, 2°C, and 3°C world, the well–established definitions are followed (King et al., 2017). The 1.5 °C/2 °C/3 °C period is determined to be the time at which the 30–year running mean is between 1.3°C/1.8°C/2.8°C and 1.7°C/2.2°C/3.2°C (crossing the 1.5 °C/2 °C/3 °C threshold) warmer than the pre–industrial levels (You et al., 2019; Zhang et al., 2018).

4. Results and discussion

4.1. Evaluation of spatial variability

To evaluate the model performance in simulating the spatial patterns of T_{min}, T_{max}, and T_{mean} over SA, we employed the Taylor diagram method (Fig. 2). In Fig. 2a, all models have shown a positive correlation coefficient with *R* values ranging from 0.23 to 0.67 for $T_{min,}$ which is greater than that of T_{max} and T_{mean}. The BCC–CSM1.1 (INMCM4) model shows the highest (lowest) *R* value of 0.67 (0.23), suggesting higher (lower) similarities with the observed dataset. Similarly, most of the models exhibit *Std* for T_{min} in the range of 1.10 to 1.50 with a maximum/minimum *Std* value of 1.90/0.89 by IPSL–CM5A–LR/CNRM–CM5 and MIROC–ESM–CHEM models. The results suggest that majority of the models exhibit relatively fair ratio of amplitude against the benchmark. The *ub*RMSD of T_{min} for most of the models were above 1 with a maximum (minimum) value of 1.63 (0.84) by IPSL–CM5A–LR (MIROC–ESM–CHEM) model, which indicates most of the models reproduced relatively higher differences against the corresponding observed data.

Fig. 2b shows the models' ability to simulate spatial patterns of T_{max} over SA. The results indicate that the correlation between each GCM simulation and observation is lower than that of T_{min} and T_{mean}, which means that the selected GFCMs exhibit least similarities to the observed T_{max} over the study region. The highest (lowest) correlation is shown by BCC–CSM 1.1 (MRI–CGCM3) model with a spatial *R* value of 0.50 (0.03). For *Std* and *ub*RMSD of Tmax, all models exhibit relatively larger magnitude of amplitude and differences than observation, indicating that Tmax is marginally simulated by CMIP5 models over the target region. Most of the models have *Std* values in the range of 1.30 to 1.70, while the values of *ub*RMSD are in the range of 1.40 to 1.70. The maximum (minimum) value of *Std*/*ub*RMSD for T_{max} is 1.93/1.87 (1.05/1.13) by CanESM2 and INMCM4 (CSIRO–MK3.6.0), representing relatively poor (better) performance against the observed data.

Similarly, the performance of models in simulating the spatial patterns of T_{mean} is shown in Fig. 2c. The results illustrate that all models display positive *R* values ranging from 0.22 to 0.62, indicating optimistic similarities in the selected model outputs against the observed data. The highest (lowest) *R* value is shown by BCC–CSM 1.1 (MRI–CGCM3) against the benchmark. Most of the models exhibit *R* values in the range of 0.30 to 0.60, indicating that CMIP5 models fairly simulate T_{mean} over the study region. In terms of *Std* of T_{mean}, most of the models display large ratio of deviations and amplitudes against the observed data ranging from 1.20 to 1.69. The results indicate that the CanESM2 (CSIRO–MK3.6.0) model has shown the highest (lowest) *Std* at the rate of 1.69 (1.01), representing weak (strong) similarities with the corresponding observed data. Similarly, the *ub*RMSD shows comparatively larger differences ranging from 1 to 1.5 with a maximum (minimum) value of 1.54 (0.97) by IPSL–CM5A–LR (CSIRO–MK3.6.0) model, which indicates that the selected GCMs have relatively large differences with respect to the observed T_{mean}.

It can be concluded that the large differences displayed by the selected models in the simulation of T_{min}, T_{max} and, T_{mean} over SA could be the result of complex topography, distinct geographical location, and diverse climatology of the region (Gusain et al., 2020; Sanjay et al., 2017; Su et al., 2016). The study region exhibits large variations in landscape and climatology ranging from complex terrains of HKH in the northern parts with a humid cold climate, flat arable plains with tropical climate in central parts and coastal belt in the south with a hot arid climate, respectively (Ahmed et al., 2019c; Alamgir et al., 2019; Bhatti et al., 2020; Im et al., 2017; Khan et al., 2018a; Sheikh et al., 2015). Moreover, the higher values of *Std* and *ub*RMSD exhibited by CMIP5 models indicate relatively higher amplitudes and larger differences for T_{min}, T_{max} and T_{mean} against the corresponding benchmarks. These deviations and discrepancies can be attributed to different physical processes and parameterization schemes of each model, which can be reduced by using the MMEM method (Kharin et al., 2013; Miao et al., 2013; You et al., 2019). It is believed that the use of MMEM is one of the effective ways to overcome the internal uncertainty of the models by generalizing the computation and improving the overall collective performance of the selected models (Janes et al., 2019; Noor et al., 2019; Su et al., 2016).

To more precisely classify the spatial performance of 21 CMIP5 models, we first calculated the three aspects (*R*, *Std*, and *ub*RMSD) of the Taylor diagram and then estimated the CRI to show a comprehensive ranking for each model. Fig. 3 illustrates the spatial ranking of each model in terms of T_{min}, T_{max}, and T_{mean} using the CRI technique. The models' simulation performance is presented in descending order. Each model is ranked from 1 (best) to 21 (worst) for T_{min}, T_{max} and T_{mean}. The ranking of the three metrics (*R*, *Std*, and *ub*RMSD) for T_{min}, T_{max}, and T_{mean} are relatively different from each other. For instance, the CSIRO–MK3–6–0 model's *R*, *Std*, and *ubRMSD*, rank values for T_{min}/T_{max}/T_{mean} are 2, 2, 1/2, 1, 1/5, 4, 2, respectively. It indicates that each model can display quite similar rank values of *R*, *Std*, and *ub*RMSD for T_{min}, but it could be different for $T_{max\ and}$ T_{mean} and so on. The model that performed best in simulating T_{min}, T_{max}, and T_{mean} over SA is CSIRO–MK3–6–0. This model is developed by Climate Change Centre of Excellence, Australia and is based on extensive meteorological observation inputs compared to other models (Collier et al., 2011). According to Fischer et al. (2014); Ahmed et al. (2020a, 2020b); Ahmed et al. (2019b); You et al. (2018), this model performs better in reproducing the spatial pattern of simulated temperature against the observed pattern. The other optimal models include; MIROC-ESM-CHEM, BCC-CSM 1-1, CNRM-CM5, and CCSM4 with better performance in spatial simulations of T_{min}, T_{max}, and T_{mean} over SA. The better performance of these models in simulating the spatial pattern of temperature and its extremes is confirmed by recent studies conducted in

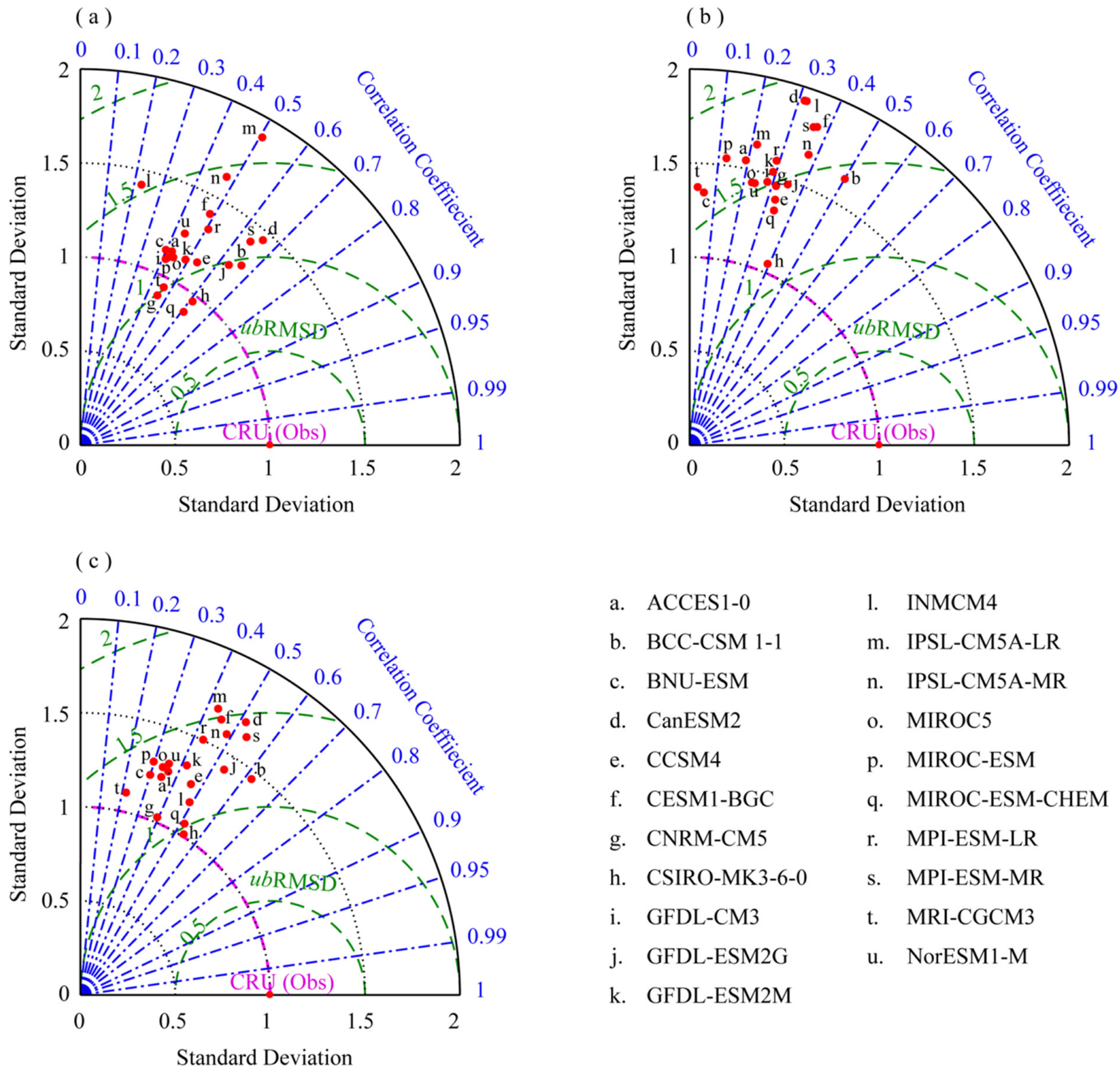

Fig. 2. Taylor diagrams of T_{min} (a), T_{max} (b), and T_{mean} (c) simulations and observations

the study area and neighboring regions (Ahmed et al., 2019b; Khan et al., 2020a, 2020b; Salman et al., 2018; You et al., 2018; Zhang et al., 2017).

4.2. Evaluation of interannual/ temporal variability

Fig. 4a shows the performance of each model in simulating the interannual variability of T_{min}, T_{max}, and T_{mean} in the study region. The model with IVS value close to 0 is considered best in capturing the skill at interannual cycles of T_{min}, T_{max}, and T_{mean}. The results indicate that CSIRO–MK3–6–0 is the best model for simulation of T_{min}, T_{max}, and T_{mean} over SA. The model gives the best result with IVS values of 0, 0.1, and 0 for T_{min}, T_{max}, and T_{mean}, respectively. Due to its optimum performance, this model is recommended by several studies for the projection of temperature and its extremes in the study region (Ahmed et al., 2019b; Ahmed et al., 2020a; Khan et al., 2020a, 2020b; You et al., 2018). In addition, the MIROC–ESM–CHEM and MRI–CGCM3 models also performed better in simulating the interannual variability of T_{min}, T_{max}, and T_{mean} with IVS values of 0.05, 0.32, 0.01 and 0.01, 0.41, 0.04, respectively. These models outperformed in the projection of climate variables in the SA and neighboring regions and are highly recommended by several researchers (Ahmed et al., 2020a; Khan et al., 2020a, 2020b; Sa'adi et al., 2020; Salman et al., 2018; Zhang et al., 2017). It is worth mentioning that the majority of the models exhibit large range in terms of simultaneous simulation of interannual variability. Overall, the lowest IVS values of individual models are calculated for T_{min} followed by T_{max} and T_{mean}, which suggest that the selected models simulate T_{min} better than T_{max} and T_{mean} in terms of interannual variability.

4.3. Overall ranking

The comprehensive rank is calculated for each model based on Taylor diagram and IVS results. The overall ranking of all models in terms of spatial and temporal performance is shown in Fig. 4b. The models are ranked in ascending order with the best to worst model. The model with the minimum score is considered as the best model. According to the overall model ranking, CSIRO–MK3–6–0 is the optimal model with an overall score of 2. This model has consistently and accurately simulated the spatial and temporal variability of T_{min}, T_{max}, and T_{mean} over SA. Several studies reported that this model is effective in the simulation of spatiotemporal characteristics of temperature and

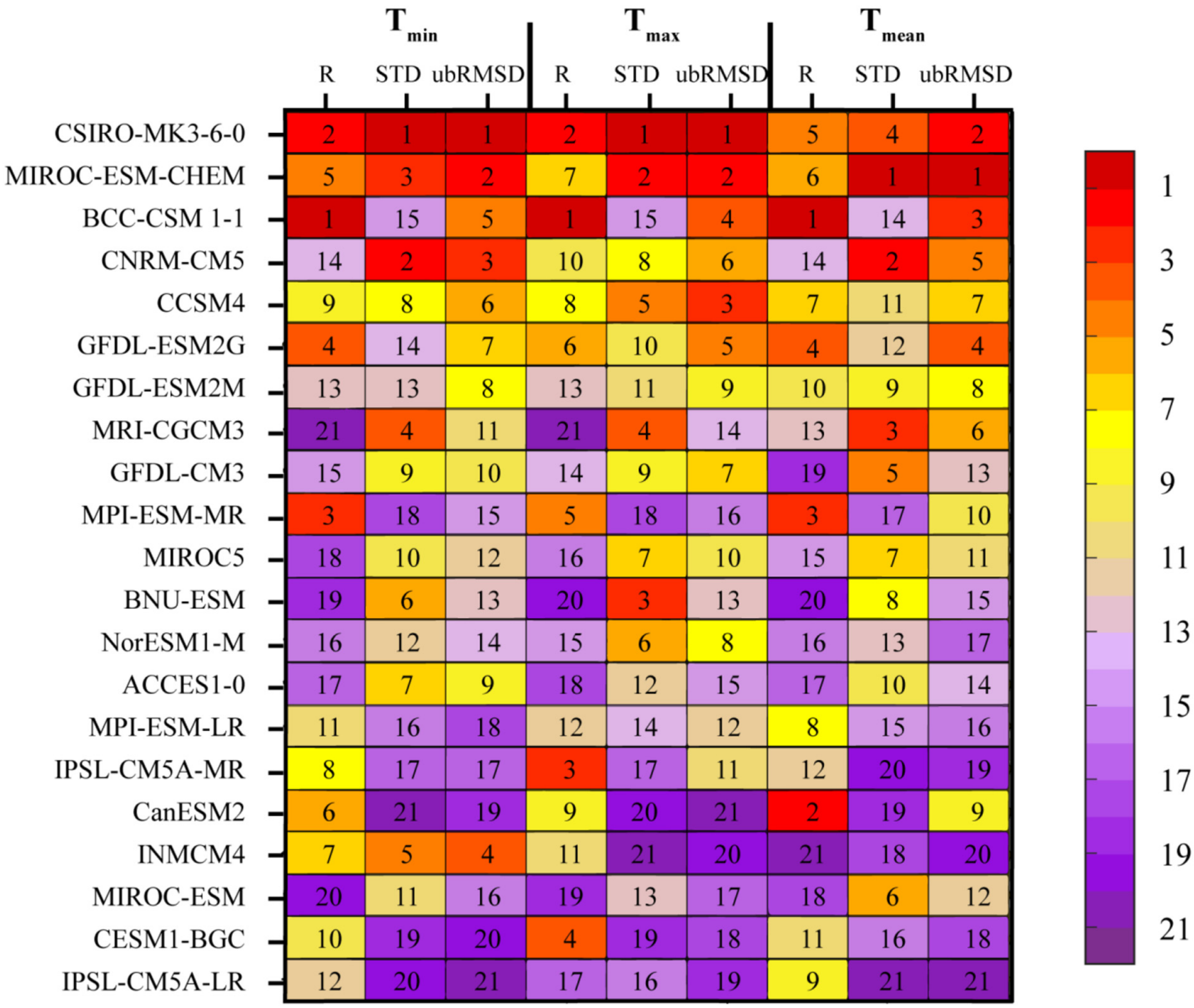

Fig. 3. Portrait diagram for T_{min}, T_{max} and T_{mean} by rank of *R*, *Std* and *ub*RMSD. Color denotes model's rank for each index.

related extremes over the study region and northern hemisphere (Ahmed et al., 2020a; Ahmed et al., 2019a; Collier et al., 2011; Fischer et al., 2014). The other models with the best performance are; MIROC–ESM–CHEM, CNRM–CM5, CCSM4, and MRI–CGCM3 with overall score of 4, 9, 11 and 11, respectively. The optimum performance of the above-mentioned models are also reported by recent studies in the simulations of temperature and its extremes over different parts of SA and surrounding regions (Ahmed et al., 2019b; Ahmed et al., 2020a; Khan et al., 2020a, 2020b; Sa'adi et al., 2020; Salman et al., 2018; You et al., 2018; Zhang et al., 2017).

4.4. Corresponding year for SA during global warming of 1.5 °C, 2 °C, and 3 °C

Fig. 5 summarizes the year in which the MMEM of 21 CMIP5 models for the SA rise by 1.5 °C, 2 °C, and 3 °C above the pre–industrial levels (as represented by the 1861–1990 baseline period) under RCP4.5 and RCP8.5 scenarios. The results indicate that warming over SA is more rapid than the global average, suggesting the earlier arrival of the corresponding year that predicted by the Paris Agreement. The earlier arrival of the corresponding years can be attributed to the increase in aerosol concentration and rise in global mean CO_2 concentration, which would certainly intensify the warming tendency of global surface and air temperature, especially in the arid and hyper-arid region of SA (Aadhar and Mishra, 2020; Ahmed et al., 2019c; Ali et al., 2020; Ramachandran et al., 2012; Xu et al., 2020). It is noteworthy that the warming targets of 1.5 °C, 2 °C, and 3 °C arrived earlier in the RCP8.5 than that of RCP4.5 for SA; however, the corresponding time periods for 1.5 °C, 2 °C, and 3 °C levels are larger in RCP4.5 than RCP8.5 scenario. On the basis of the 30–year running mean of MMEM, the RCP4.5 scenario predicts that the 1.5 °C target will reach by 2006–2027 (2019), which is slightly later than the arrival anticipated by RCP8.5 scenario, i.e., 2006–2024 (2016). The results are in agreement with the findings of previous studies focusing on SA and adjoining regions (Khan et al., 2020a, 2020b; Mishra et al., 2017; Xu et al., 2017; Yaduvanshi et al., 2019; Zhang et al., 2017).

Similarly, the RCP4.5 scenario projects that the 2 °C warming target will occur during 2028–2044 (2036), almost 6 years later than for RCP8.5 scenario, which projects that the 2°C warming will reach during 2025–2036 (2030). These warming years are in the range of recent studies conducted in the study region and around the globe (Yaduvanshi et al., 2019; You et al., 2019; Zhang et al., 2018). Furthermore, the 30–year running average of MMEM temperature for SA estimates that the 3 °C warming target under RCP4.5 scenario will reach in 2062–2099 (2074), nearly 24 years later than for RCP8.5 scenario, which anticipates that the 3 °C will occur from 2046–2054 (2050). These results are in the range of findings reported by previous studies (Liu et al., 2018; Zhang et al., 2018). The overall analysis suggests that SA will be highly influenced by global warming in the future, as the corresponding years for 1.5 °C, 2 °C, and 3 °C warming targets over SA arrive earlier than global level. This earlier arrival of the corresponding years for the selected warming levels would result in

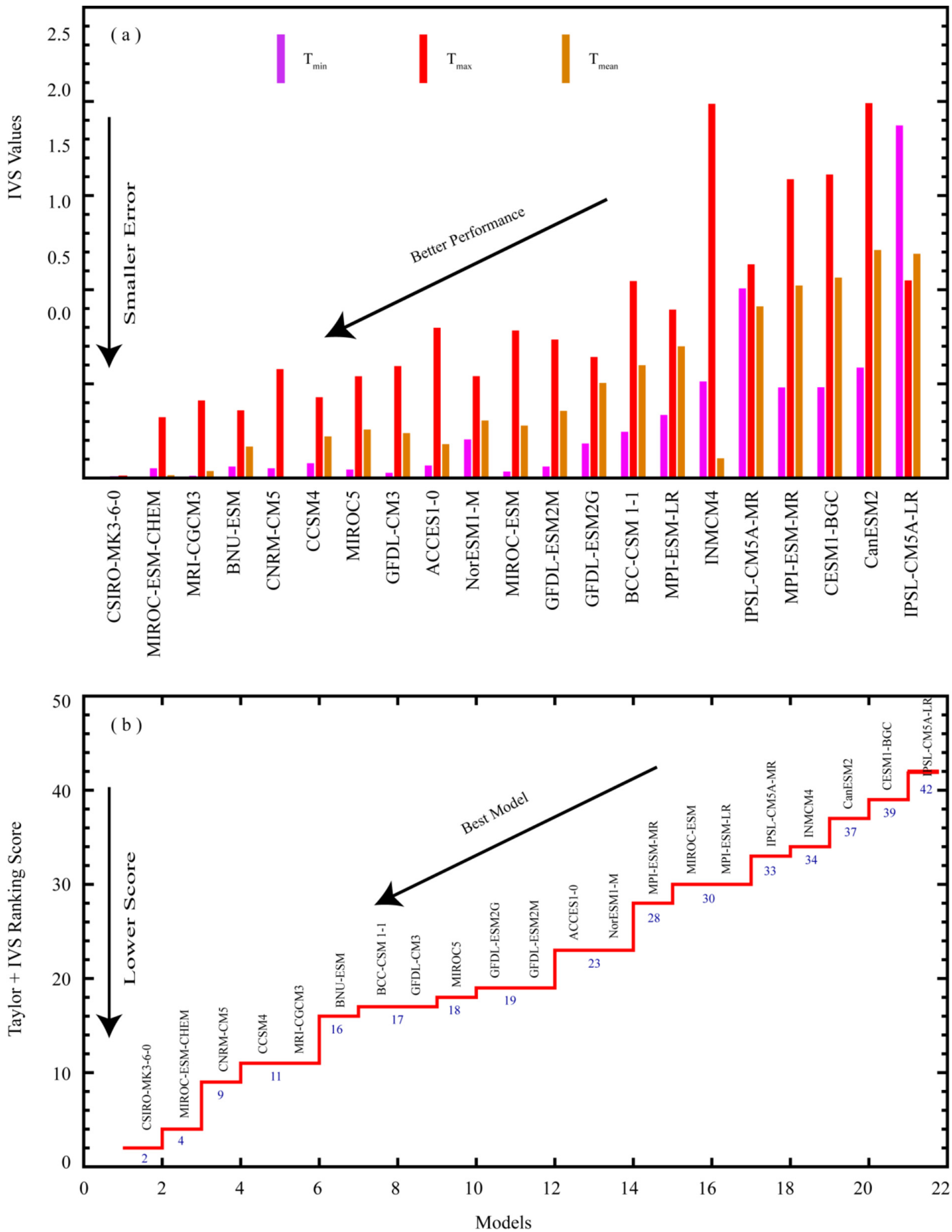

Fig. 4. The IVS and Comprehensive models ranking for T_{min}, T_{max} and T_{mean} over SA; (a) IVS (Temporal) skill scores of models. The IVS closer to zero indicates better model performance. (b) Comprehensive models ranking based on spatial and temporal skills score. The number below each model indicates the overall score of the model. The model with low score indicates better performance.

intense, frequent, and prolonged temperature extremes with large geographical extent over SA in the near future (Aadhar and Mishra, 2020; Khan et al., 2020a, 2020b; Mishra et al., 2017; Ullah et al., 2019b).

4.5. Changes in temperature under global warming of 1.5 °C, 2 °C, and 3 °C

Table 2 represents the changes in regionally averaged MMEMs T_{min}, T_{max}, and T_{mean} under global warming targets of 1.5 °C, 2 °C, and 3 °C

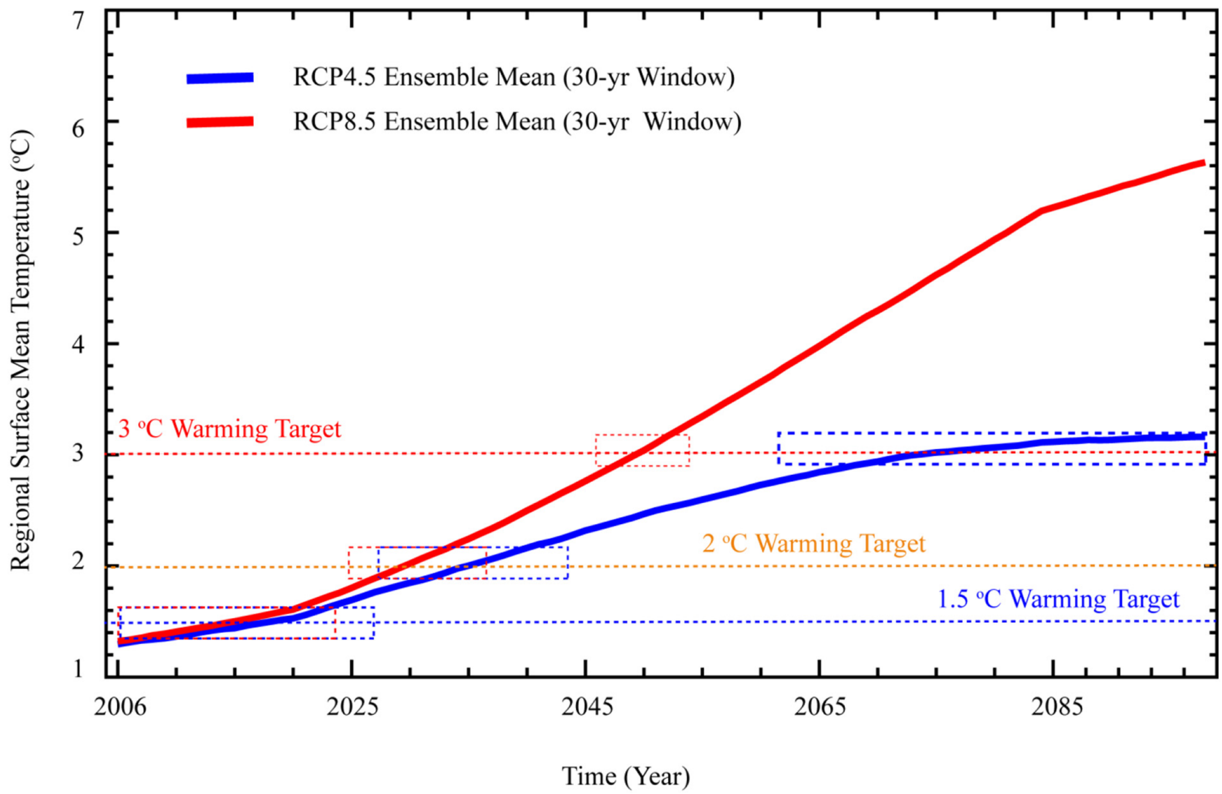

Fig. 5. Regionally averaged mean surface temperature for SA during 2006-2100 from 21 CMIP5 models ensemble mean under RCP4.5 and RCP8.5 scenarios. The blue/red rectangle boxes on the two RCPs indicate the ensemble mean projection targets of 1.5°C, 2°C and 3 °C above pre-industrial levels (as represented by the 1860-1880 baseline period).

Table 2
Changes in regionally averaged MMEMs T_{min}, T_{max}, and T_{mean} for SA during 1.5 °C, 2 °C, and 3 °C global warming targets with respect to the pre–industrial levels (1861–1880) under RCP4.5 and RCP8.5 scenarios.

Temperature	RCP4.5 scenario			RCP8.5 scenario		
	1.5 °C	2 °C	3 °C	1.5 °C	2 °C	3 °C
T_{min}	1.53	2.18	3.18	1.52	2.20	3.20
T_{max}	1.28	1.91	2.97	1.26	1.85	2.79
T_{mean}	1.40	2.03	3.06	1.39	2.01	2.97

for RCP4.5 and RCP8.5 scenarios with respect to the pre–industrial levels. Corresponding to 1.5 °C, 2 °C, and 3 °C thresholds, the MMEM T_{min} over SA will increase by 1.53°C, 2.18°C, and 3.18°C under RCP4.5 scenario above the pre–industrial levels, respectively. The analysis further illustrates that SA will experience a rise in MMEM T_{max} under the warming targets of 1.5 °C, 2 °C, and 3 °C by 1.28°C, 1.91°C, and 2.97°C for RCP4.5 scenario, respectively. For MMEM T_{mean}, increases of 1.40°C, 2.03°C, and 3.06°C are projected over SA in response to 1.5 °C, 2 °C, and 3 °C warming levels under the RCP4.5 scenario, respectively. The results are in agreement with the findings of You et al. (2019), who reported 2.11°C and 2.89°C increase in T_{mean} over the Tibetan Plateau for RCP4.5 scenario under the warming levels of 1.5 °C and 2 °C, respectively. In another study, Wu et al. (2020) estimated an increase of 2.11°C and 2.96°C in T_{mean} for RCP4.5 scenario over the Tibetan Plateau at 1.5 °C and 2 °C warming levels, respectively. Yaduvanshi et al. (2019) projected an increase of 1.4 – 2.1°C T_{mean} over different parts of India under RCP4.5 scenario at 1.5 °C and 2 °C warming levels. It should be noted that the northwestern domain of SA is an integral part of the Tibetan Plateau, which is already experiencing significant warming and is expected to experience more warming in the future.

Similarly, for RCP8.5 scenario, the analysis anticipated a sharp increase in MMEM T_{min} over SA by 1.52°C, 2.20°C, and 3.20°C under 1.5 °C, 2 °C, and 3 °C warming thresholds above the pre–industrial levels, respectively. The T_{max} analysis indicates that the region will experience a warming trend over SA at the rate of 1.26°C, 1.85°C, and 2.79°C for 1.5 °C, 2 °C, and 3 °C thresholds, respectively. Moreover, the MMEM T_{mean} under RCP8.5 scenario predicts increases of 1.39°C, 2.01°C and 2.97°C over the target region in response to 1.5 °C, 2 °C, and 3 °C warming levels, respectively. These results are in the range of warming reported by Khan et al. (2020a, 2020b), with an increase of 0.54 – 4.17 and 0.69 – 4.55°C in T_{min} and T_{max} over Bangladesh at 1.5 °C 2 °C, and 4 °C warming levels under RCP8.5 scenario, respectively. According to Yaduvanshi et al. (2019), India is likely to experience a rise in T_{mean} at rate of 1.9 – 2.8°C during RCP8.5 scenario at 1.5 °C and 2 °C warming thresholds relative to the pre-industrial period. Similarly, Sanjay et al. (2017) projected a rise of 5.4°C and 4.9°C warming in winter and summer temperature over different parts of SA by the end of 21st century under RCP8.5 scenario. Although their reported changes are higher than that of the present studies; however, they did not consider any warming levels and the estimated changes are reported for the whole century.

It is worth-mentioning that RCP4.5 scenario projects greater changes in temperature over SA for all warming targets than RCP8.5 scenario; however, in case of T_{min}, RCP8.5 scenario predicts higher changes in 2 °C and 3 °C warming levels than that of RCP4.5 scenario. The higher changes in RCP4.5 scenario could be the result of the late arrival of the 1.5 °C, 2 °C, and 3 °C warming levels and extended corresponding periods for all warming targets over SA. As several reported that the global mean temperature is getting warmer with passage of time with highest increase by the end of the 21st century. In a recent studies, You et al. (2019); Wu et al. (2020); Yaduvanshi et al. (2019) also reported similar results for Tibetan Plateau and India, indicating more warming under RCP4.5 than RCP8.5 scenario. Generally, the findings suggest that there is a sharp rise in SA temperature under global warming trends, which will continue in the future with more drastic impacts (Cheng et al., 2012; Rehman et al., 2018; Saeed et al., 2017; Sheikh et al., 2015; Ullah et al., 2019a). The rise in temperature would increases melting of snow and glaciers in the Himalayas, causing severe flooding in the near future and drought in the far future over the Indus, Ganges, and Brahmaputra river basins (Almazroui et al., 2020; Bocchiola and Diolaiuti, 2013; Das and Meher, 2019; Janes et al., 2019; Sanjay et al., 2017). Eventually, the subsequent hydrometeorological calamities would potentially trigger extensive displacement and migration of millions of people into already highly populated regions, resulting in increased pressure on local water and land resources (Aadhar and Mishra, 2019; Yadav and Lal, 2018; Yaduvanshi et al., 2019). The higher warming tendency of temperature and its extremes over SA is closely linked to the high population density, rapid urbanization, increasing concentration of aerosols and CO_2 in the region (Ali et al., 2020; Ravi Kumar et al., 2016; Ullah et al., 2018b; Xu et al., 2020). Moreover, the intensification of future temperature and its extremes is expected to be high over the target region due to dynamic variability of the related climatic factors including, precipitation, potential evapotranspiration, cloud cover, soil moisture, air temperature, and humidity etc., (Aadhar and Mishra, 2020; Ahmed et al., 2020b; Wehner et al., 2016; Wu et al., 2020; Zhou et al., 2020).

Fig. 6 represents the range and distribution of T_{min}, T_{max}, and T_{mean} anomalies under global warming of 1.5 °C, 2 °C, and 3 °C thresholds. The interquartile models of T_{min}, T_{max}, and T_{mean} over SA have shown significant changes during the mentioned targets under RCP4.5 and RCP8.5 scenarios. The results show that T_{min}, T_{max}, and T_{mean} exhibit much larger values than the median for most of the warming levels, which imply that intense warming pattern will be sustained over the study region under both emission scenarios. The results further indicate that the increasing tendencies of T_{min}, T_{max}, and T_{mean} under 1.5 °C, 2 °C, and 3 °C warming thresholds are mostly associated with high range of values of the corresponding temperature over SA. From the results, it can be concluded the larger range of interquartile model for T_{min}, T_{max}, and T_{mean} may affect the frequency, intensity, and duration of temperature extremes in the study region. These changes are in line with the warming pattern projected in the spatial distribution of temperature during 1.5 °C, 2 °C, and 3 °C thresholds. Similar distribution of T_{min}, T_{max}, and T_{mean} is reported by Wu et al. (2020); You et al. (2019) over the Tibetan Plateau for different warming levels under RCP4.5 and RCP8.5 scenarios. Moreover, the results are also consistent with the radiative forcing trajectories included in the representative concentration pathways of the CMIP5 models (Moss et al., 2010; Taylor et al., 2012).

4.6. Spatial patterns of 1.5 °C, 2 °C, and 3 °C warming targets

Fig. 7 shows the spatial distribution of surface T_{min}, T_{max} and T_{mean} changes from MMEMs over SA at a global warming level of 1.5 °C. The MMEMs of T_{min}, T_{max}, and T_{mean} under RCP4.5 and RCP8.5 scenarios indicate that the warming pattern increases over SA for 1.5 °C warming target relative to the pre–industrial levels. It has been found that T_{min} increases at a faster rate than T_{max} and T_{mean} under both emission scenarios; however, the warming rates of T_{min} under RCP4.5 scenario are higher than the RCP8.5 scenario. The asymmetrical pattern of T_{min}, T_{max}, and T_{mean} suggests that the study region is likely to face significant warming in the future with dynamic fluctuations in cold and warm temperature extremes (Dimri et al., 2018a, 2018b; You et al., 2019). This uneven pattern of T_{min}, T_{max}, and T_{mean} would have adverse effects on the biodiversity, water resources, and agriculture production of the study region (Khan et al., 2020a, 2020b; Yaduvanshi et al., 2019). Moreover, these heterogeneous patterns may affect the seasonal cycle of the region due to which severe, concurrent, and prolonged daytime and nighttime extreme events are expected to occur in the future with substantial effects (Abbas et al., 2018; Panda et al., 2017; Ullah et al., 2019b).

The changes in T_{min}, T_{max}, and T_{mean} under both scenarios exhibit high spatial variability with the obvious warming in the northwestern parts of SA i.e., HKH region. Under both scenarios, the changes in T_{min}, T_{max}, and T_{mean} over high latitudes are projected to be increased at the rate of 2.1°C, 1.8°C, and 1.9°C above the pre–industrial levels, respectively. These results affirm the findings of Yaduvanshi et al. (2019), who reported an increase of 2°C in T_{mean} over northwestern India under 1.5 °C warming world. The results further support the findings of Dimri

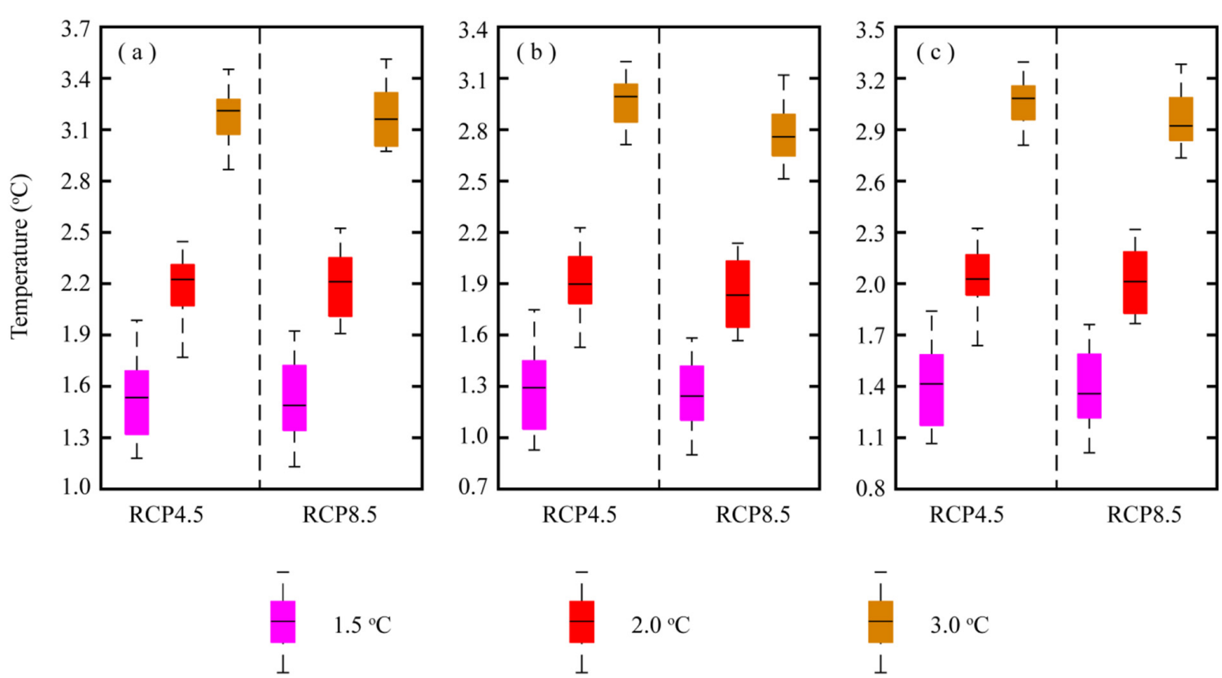

Fig. 6. Range (lowest to highest) of projected changes in T_{min}, T_{max}, and T_{mean} with respect to the pre–industrial levels (1861–1880); (a) T_{min}, (b) T_{max}, and (c) T_{mean}. The upper and lower hinges of each box and whisker plot represent the 25th and 75th percentile. The central black line of each box and whisker indicates the median value.

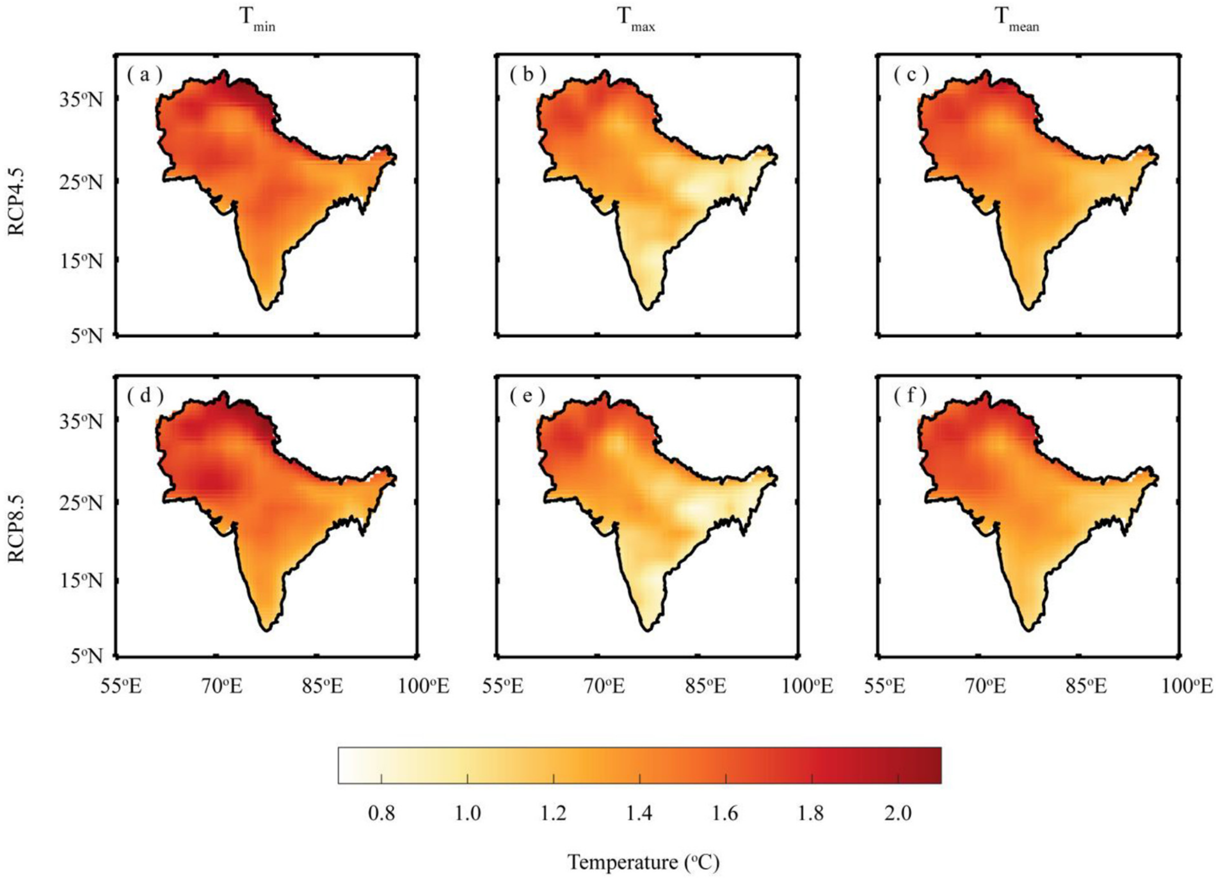

Fig. 7. Spatial distribution of T_{min}, T_{max}, and T_{mean} from 21 CMIP5 models ensemble mean over SA under RCP4.5 (a, b, c) and RCP8.5 (d, e, f) scenarios at a global warming of 1.5 °C above the pre–industrial levels (1861–1880).

et al. (2018); Dimri et al. (2018b), who projected significant warming in seasonal T_{min}, T_{max}, and T_{mean} over the Indian Himalayan region at the rate of 0.23 − 0.90°C per decade under RCP4.5 and RCP8.5 scenarios. Similarly, the outputs from CMIP5 and CMIP3 also estimated an increase of 2.5–4°C and 2.8–4.5°C in T_{mean} over eastern and western Himalayan regions by the end of 21st century, respectively (Panday et al., 2014). Dash et al. (2012) projected an increase of 0.64–5.15°C in annual T_{mean} over eastern Himalayan region by the end of the 21st century. According to Rajbhandari et al. (2015), the upper parts of the Indus River basin is expected to experience significant warming in the future within the range of 0.5–2.0°C and 2.2–5.8°C under RCP4.5 and RCP8.5 scenarios during 2006–2100, respectively.

The central and southern regions of SA such as southwestern (southeastern) India (Pakistan) will experience a moderate increase in the warming pattern of T_{min}, T_{max}, and T_{mean} under RCP4.5 (RCP8.5) scenario, with an estimated rate of 1.9°C, 1.4°C, and 1.6°C (2°C, 1.3°C, and 1.5°C) above the pre–industrial levels, respectively. These results are in agreement with the findings of previous studies covering the said regions (Janes et al., 2019; Rajbhandari et al., 2015; Su et al., 2016). Recently, Yaduvanshi et al. (2019) projected a gentle rise in temperature at the rate of 1.7–2.2°C and 1.2–1.9°C for 1.5 warming level under RCP4.5 and RCP8.5 scenarios with respect to the pre-industrial level. According to Zheng et al. (2018), the median projection of seasonal and annual temperature over the central and southern SA show an increase of 2–2.3°C for RCP8.5 by 2046–2075 relative to the baseline period (1976–2005). Similarly, Rajbhandari et al. (2015) indicated that the lower parts of the Indus Basin covering the central and southern SA are expected to experience significant warming in winter T_{min} and summer T_{max} at the rate of 1.5–3.5°C and 1–3°C for A1B scenario during 2011–2098 relative to the baseline period (1961-1960), respectively. The warming pattern of temperature suggests that these regions may experience frequent and intense temperature extremes such as heat waves, heat stress, and drought in the near future (Im et al., 2017; Mazdiyasni et al., 2017). Several studies based on observational and remote sensing data have reported severe heatwaves and drought events in the said regions over the recent past (Ahmed et al., 2018; Khan et al., 2018b; Ullah et al., 2019b; Wehner et al., 2016), which highlights their degree of vulnerability to climate change and climate extremes in the current and future scenarios.

Furthermore, the analysis reveals that the rest of SA (eastern India, Bangladesh, and Nepal) exhibits a slight increase in T_{min}, T_{max}, and T_{mean} under RCP4.5 (RCP8.5) scenario at the rate of 1.2°C, 0.8°C, and 1.1°C (1°C, 0.7°C, and 1°C) above the pre–industrial levels, respectively. The projected changes are in the range reported by previous studies (Mishra et al., 2017; Xu et al., 2017). Our findings support the range of temperature changes reported by Khan et al. (2020a, 2020b), with a rise of 0.69 − 1.44°C and 0.54 − 1.45°C in seasonal T_{min} and T_{max} over Bangladesh for RCP8.5 under global warming of 1.5 °C relative to the present world, respectively. Similarly, these results in line with the warming rates suggested by Yaduvanshi et al. (2019) for eastern India under 1.5 °C global warming level relative to the pre-industrial level. They reported that the eastern parts are subjected to the lowest warming with an estimated increase of 1.2 − 1.9°C and 1.2 − 1.7°C under RCP4.5 and RCP8.5 scenarios, respectively. Our results further strengthened by the rate of warming projected by Cuba et al. (2017) over the eastern state of India, i.e., Tamil Nadu. They projected a slight warming in the said region at the rate of 0.15°C and 0.37°C (0.13°C and 0.34°C) for T_{min} (T_{max}) during RCP4.5 and RCP8.5 scenarios by the end of the 21st century relative to the baseline period (1971-2000), respectively. Similarly, many studies anticipated minor changes in

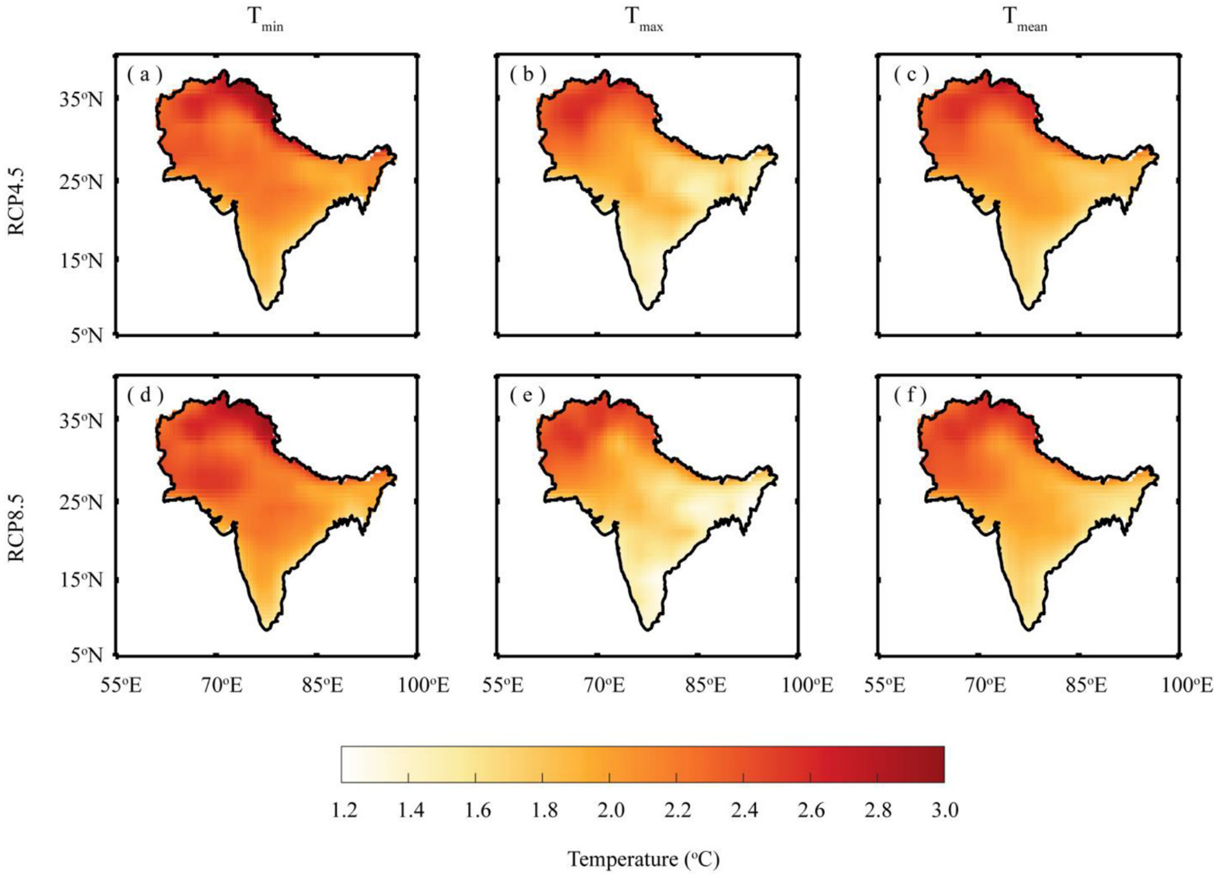

Fig. 8. Similar to Fig. 7, but for a global warming of 2 °C

temperature extremes over the eastern parts of SA under 1.5 °C warming level, which can be attributed to the lower warming tendency of temperature and high intensity of precipitation in the region (Aadhar and Mishra, 2020; Aadhar and Mishra, 2019).

Fig. 8 represents the spatial pattern of MMEMs of T_{min}, T_{max}, and T_{mean} over SA under 2 °C warming target for RCP4.5 and RCP8.5 scenarios relative to the pre–industrial levels. The spatial analysis of T_{min}, T_{max}, and T_{mean} shows a prominent rise in the warming pattern under RCP4.5 and RCP8.5 scenarios. Similar to 1.5 °C, the increase in T_{min} is greater than T_{max} and T_{min} during 2°C under RCP4.5 and RCP8.5 scenarios. This indicates their asymmetric warming patterns in the future, which would have adverse impacts on the hydrological, agricultural and ecological setups of the study region (Sanjay et al., 2017; You et al., 2019). Moreover, the uneven warming tendency of T_{min}, T_{max}, and T_{mean} would result in decreasing diurnal temperature range (Dimri et al., 2018a; You et al., 2017a, 2017b), which would certainly significantly affect the seasonal cycle of the region by changing the cold season and moderate seasons into more warm seasons (Fowler and Archer, 2006; Gu et al., 2012; Naveendrakumar et al., 2019). Similarly, this may result in maximum number of daytime and nighttime temperature extremes in the future over the study region (Alamgir et al., 2019; Mahmood et al., 2015; Su et al., 2016).

The estimated changes in T_{min}, T_{max}, and T_{mean} show high spatial variability under both emission scenarios. It is worth–mentioning that T_{min} experiences a sharp increase under RCP8.5 scenario, while T_{max} exhibits strong warming under RCP4.5 scenario. The maximum (minimum) increase in T_{min}, T_{max}, and T_{mean} will be found over the northwestern (eastern) parts of SA. Under RCP4.5 (RCP8.5) scenario, the intensity of T_{min}, T_{max}, and T_{mean} during 2°C warming threshold over the northern and western parts is projected to be increased by 3°C, 2.6°C, and 2.8°C (3°C, 2.8°C, and 2.8°C) above the pre–industrial levels. The results are in agreement with the findings of Yaduvanshi et al. (2019), who reported an increase of 2.1°C in T_{mean} over northwestern parts of India at 2.0 °C warming threshold. The results further affirm the findings of Xu et al. (2017), who suggested that the temperature over SA will increase by $2.1-2.4$°C with maximum intensity in the high altitudes under 2 °C, compared to the pre-industrial era. According to You et al. (2019), the southern parts of Tibetan Plateau covering the HKH region is expected to experience a warming tendency of $3.2-3.4$°C, $3.0-3.2$°C, and $2.8-3.0$°C in T_{min}, T_{max}, and T_{mean} at 2 °C warming level under both emission scenarios, respectively; however, the warming rate is likely to be high under RCP4.5 than RCP8.5 scenario for all variables. Similarly, the temperature over the HKH region of Tibetan Plateau will reach to 2.96°C and 2.85°C for RCP4.5 and RCP8.5 scenarios relative to the pre-industrial period, respectively (Wu et al., 2020). Our results also support the warming rate reported by Gu et al. (2012), who employed high resolution downscaled model over the study region. They projected an increase of $3-4$°C in annual and seasonal temperature over the northwestern parts of SA. Similarly, Panday et al. (2014) projected a rise of 2.5–4°C and 2.8–4.5°C in the eastern and western Himalayas by 2100.

The central parts of SA such as western India and eastern Pakistan exhibit a gentle rise in T_{min}, T_{max}, and T_{mean} by 2.6°C, 1.8°C, and 2°C (2.7°C, 1.9°C, and 2.1°C) under RCP4.5 (RCP8.5) scenario, respectively. The results are in agreement with the findings of recent studies. For instance, Yaduvanshi et al. (2019) estimated an increase of 2.2–2.8°C and 2.2–2.9°C in annual T_{mean} over the western parts of India under 2 °C warming target for RCP4.5 and RCP8.5 scenarios, respectively. Similarly, Su et al. (2016) projected a notable increase in temperature over the lower Indus basin without considering the global warming targets. They stated that the target region is likely to experience a rise of 1–1.5°C and 2–2.4°C (1.5–2.5°C and 2.8–4.2°C) under

RCP4.5 (RCP8.5) scenario during 2046–2065 and 2081–2100 relative to 1986–2005, respectively. This part of SA is under the effect of high temperature with recurrent heatwaves in the past (Khan et al., 2018b; Ullah et al., 2019b; Wehner et al., 2016). It is also projected the increasing tendency of temperature may trigger severe, frequent and prolonged heatwaves in this region (Im et al., 2017; Nasim et al., 2018; Saeed et al., 2017).

Similar to 1.5 °C warming target, the eastern parts of SA will experience a slight increase in T_{min}, T_{max}, and T_{mean} under 2 °C warming level during RCP4.5 (RCP8.5) at the rate of 1.4°C, 1.3°C, and 1.4°C (1.5°C, 1.2°C, and 1.4°C), which is in the range findings reported by previous studies (Xu et al., 2017; You et al., 2019). Similar to 1.5 °C warming level, this part of SA has the lowest rate of projected warming in all temperature variables for emission scenarios. In a recent study, Khan et al. (2020a, 2020b), who projected a rise of 1.14 − 2.67°C (0.98 − 2.24°C) in seasonal T_{min} (T_{max}) over Bangladesh for RCP8.5 scenario under 2 °C global warming target. Similarly, You et al. (2019) estimated an increment in T_{min}, T_{max}, and T_{mean} at the rate of 2.0 − 2.6°C in the southeastern parts of Tibetan Plateau under 2 °C warming level relative to the pre-industrial era. It is vital to mention that the southeastern parts of Tibetan Plateau are bordering the eastern parts of SA. Though, the tendency of projected changes in this region is lower than the rest of SA, yet the impacts of climate-induced extremes would be unavoidable due to its socioeconomic convictions and geographical location (Aadhar and Mishra, 2019; Cuba et al., 2017). The region has a long coastal belt and the economy of the local people is based on fisheries and agriculture, which are highly vulnerable to climate change (Pervez and Henebry, 2015; Roy et al., 2007; Shahid et al., 2016; Yadav and Lal, 2018).

Fig. 9 summarizes the spatial distribution of T_{min}, T_{max}, and T_{mean} over SA under 3 °C warming threshold. Correspondence to the pre–industrial levels, the study region experiences a notable warming pattern during 3 °C warming target under the two emission scenarios; however, the warming pattern is more evident in the RCP4.5 scenario than RCP8.5 scenario. Similar results were reported by You et al. (2019) over the southern Tibetan Plateau, where maximum warming rate was estimated under RCP4.5 than RCP8.5 scenario. Similar to 1.5 °C and 2 °C warming targets, the T_{min} in 3 °C level increases at a faster rate than T_{max} and T_{mean} under both scenarios. This indicates that T_{min}, T_{max}, and T_{mean} would increase asymmetrically with extended hot periods and substantial nighttime extreme events in the future.

The spatial distribution of projected changes in T_{min} (T_{max} and T_{mean}) under 3 °C warming level indicates that the northern (western) parts of SA will experience a significant increase in temperature, which implies that the elevated parts of SA will be under high risk of climate change in the coming decades. The maximum changes predicted over northwestern parts of SA are at the rate of 4.2°C, 4.2°C, and 4.2°C (4.2°C, 4°C, and 4.2°C) for T_{min}, T_{max}, and T_{mean} under RCP4.5 (RCP8.5) scenario, respectively. Although the study region is expected to experience significant warming at 3 °C warming level, yet little attention has been given to it due to which we have limited literature regarding the warming tendency of temperature and its extremes over SA in 3 °C warming world. Recently, Xu et al. (2017) projected a sharp increase of 4.0 − 4.4°C in annual T_{mean} over SA with maximum rate in the higher altitude characterized by the HKH region under 3 °C warming relative to the pre-industrial level. According to Guo et al. (2017), the Xinjiang and Southern China parts bordering the northwestern South Asia are likely to experience heat waves with greater frequency and severity under RCP4.5 and RCP8.5 scenarios of 3 °C warming world. Similarly, Wang et al. (2017a, 2017b) reported higher warming rate of temperature extremes with increasing tendency of warm extremes and decreasing tendency of cold extremes across the

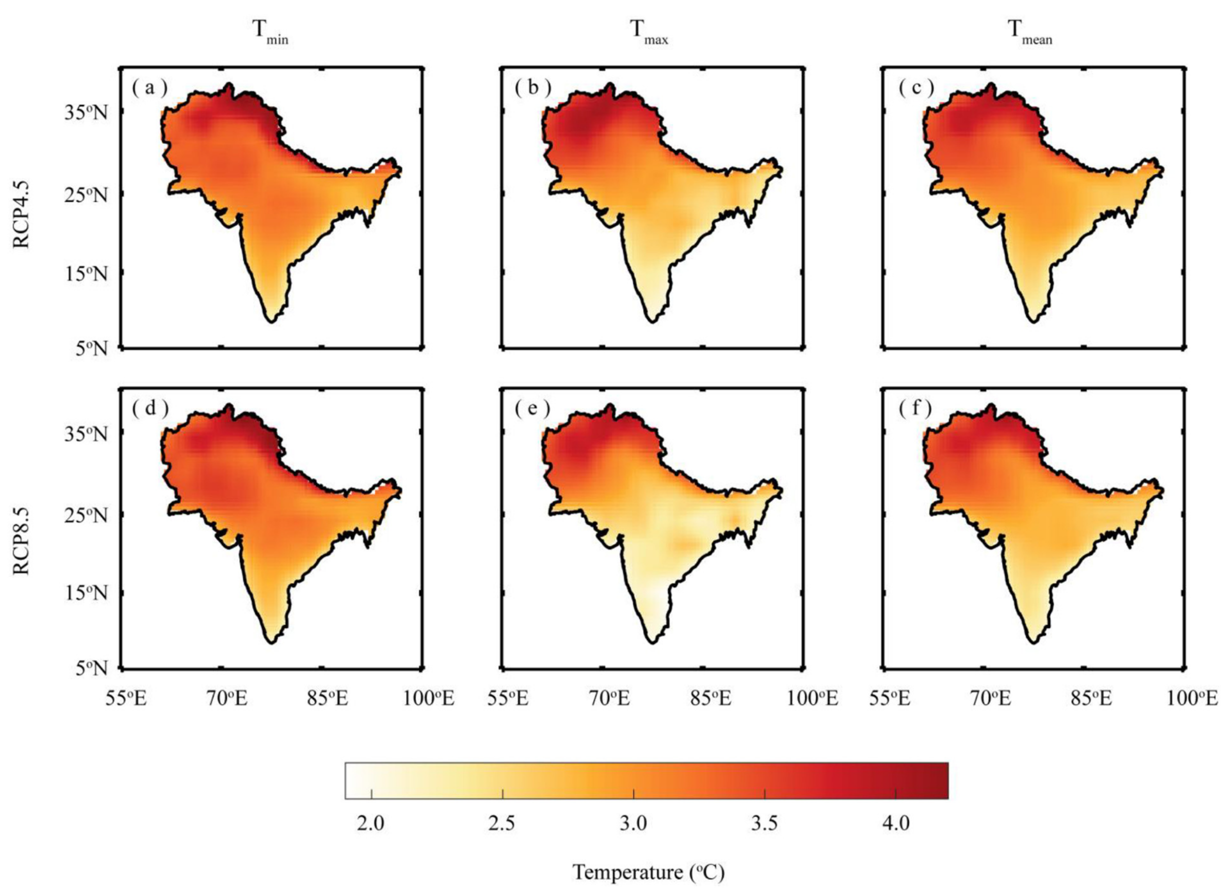

Fig. 9. Similar to Fig. 7, but for a global warming of 3 °C

world.

Similarly, the central and southern regions of SA will experience an increase of 3.8°C, 3°C, and 3.2°C (3.9°C, 2.7°C, and 2.9°C) in T_{min}, T_{max}, and T_{mean} under RCP4.5 (RCP8.5) scenario relative to the pre–-industrial levels, respectively. The results are in line with the findings of recent studies conducted in neighboring countries and regions. According to Wang et al. (2017a, 2017b), a 3 °C warmer world would feature a decrease in cold indices and an increase in warm indices with noticeable warming tendency in T_{min} based indices than T_{max} over arid and semi-arid regions of the world. Similarly, You et al. (2020) stated that the warming tendency of temperature and its extremes is expected to be amplified over different parts of the world with maximum rate in Tibetan Plateau under 3°C global warming scenario. Guo et al. (2017) indicated that the plain areas of China having similar climate like central SA, would experience severe and frequent heatwaves during RCP4.5 and RCP8.5 scenarios in 3 °C warming target above the pre-industrial level.

Moreover, under 3°C warming threshold, the eastern parts of SA exhibit slight warming in T_{min}, T_{max}, and T_{mean} with a similar spatial pattern to that of 1.5 °C and 2 °C warming targets. The projected changes in T_{min}, T_{max}, and T_{mean} over eastern SA are recorded at the rate of 2.3°C, 2°C, and 2.1°C (2.2°C, 1.9°C, and 2.1°C) under 3 °C warming level during RCP4.5 (RCP8.5) scenario, respectively. These results are in the range of findings reported by previous studies (Xu et al., 2017; Zhang et al., 2018). According Khan et al. (2020a, 2020b), the eastern parts of SA, i.e., Bangladesh would expect an increase of 2.67 − 4.55C and 2.45 − 4.17°C in T_{min} and T_{max} under RCP8.5 scenario of 4 °C warmer world. Similarly, Aadhar and Mishra (2020); Aadhar and Mishra (2019); Mishra et al. (2017); Yaduvanshi et al. (2019) projected slight changes in future temperature and its extremes over the eastern parts of SA under different global warming targets. Though it is found that the eastern parts of SA will experience slight increase in temperature under 3 °C warming level; however, these parts are highly prone to climate extremes due to their geographical location and socioeconomic conditions (Ratnam et al., 2016; Sharma et al., 2016). A mild increase in temperature is highly critical for the region and may affect the local population at large in the future.

The overall analysis suggests that SA will experience greater changes in T_{min}, T_{max}, and T_{mean} with increasing global warming thresholds under both emission scenarios. However, it has been found that climate changes associated with global warming of 1.5 °C, 2 °C, and 3 °C targets have shown non–linear responses over different parts of SA, which may have adverse effects on the local population. Moreover, the projected changes in T_{min}, T_{max}, and T_{mean}, will be stronger over higher latitude than mid–low latitude, which implies that the northwestern and central–southern parts will be adversely affected by climate change. In recent studies, it has been stated that mountainous regions are highly sensitive to climate change than other topographic classes (Pepin et al., 2015; You et al., 2019). The higher warming tendency is closely linked to the elevation–dependent warming, which highly is evident in the HKH region and is expected to increase in the future under different global warming targets (Guo et al., 2016; Khan et al., 2015; Rangwala and Miller, 2012). This sharp rise in temperature will intensify the snow and glacier melting process in the region, which may affect the water resources and the region may face flooding and drought in the coming decades (Khan et al., 2015; Kraaijenbrink et al., 2017). The increasing risks of floods and drought may affect millions of people living in the deltaic regions of Indus, Ganga and Brahmaputra rivers (Aadhar and Mishra, 2020; Almazroui et al., 2020; Yaduvanshi et al., 2019). Literature indicated that these river basins are characterized by fertile arable land with extensive agriculture production and is highly vulnerable to the adverse impacts of climate change (Ahmad et al., 2014, Ahmad et al., 2014; Mahmood and Jia, 2016). The rising tendency of temperature may affect the production of wheat, paddy, soyabean, groundnuts, and vegetables by 3–7% for everyone degree increase in temperature over the said regions (Yadav and Lal, 2018; Yaduvanshi et al., 2019).

The central parts of SA are characterized by urbanized and major metropolitan cities with dense population (Naveendrakumar et al., 2019; Sheikh et al., 2015). Moreover, the Asia famous Thar Desert is located in this part of SA, which is among the hottest regions of the world (Sun et al., 2017; You et al., 2017a, 2017b). In the present climate, this part of SA is regularly experiencing hot days, which is expected to be continued in the future with more drastic impacts (Khan et al., 2018b; Khan et al., 2020a, 2020b; Nasim et al., 2018; Saeed et al., 2017; Ullah et al., 2019b). The arid and hyper-arid climates of the region coupling with high temperature may affect the intensity, frequency, duration, and extent of the future temperature extremes (Ahmed et al., 2019c; Ullah et al., 2018b). It has been reported that the rapid urbanization, extended population and massive industrialization in the region may intensify the emission of greenhouse gasses, which ultimately alter the phenomena of global warming (Haq et al., 2017; Ullah et al., 2018b; Xu et al., 2020). Similarly, the southern parts are covered by the coastal belt, which would receive significant moisture content from the Indian Ocean (Jhajharia et al., 2009; Pathak et al., 2017b; Ullah et al., 2019b). The moving of moisture content from the source to the adjoining coastal region increases the concentration of humidity, which combines with high temperature and result in humid heatwaves over the said regions with extensive human and socio-economic losses (Fischer, 2014; Jhajharia et al., 2012; Wehner et al., 2016).

The eastern parts of SA are considered to be highly prone to the climate extremes due to their geographical location and socioeconomic conditions (Pervez and Henebry, 2015; Revadekar et al., 2013). These parts of SA are bordering with of India Ocean and Bay of Bengal having hot and dry climate. Moreover, the regional economy is mainly dependent on natural resources such as agriculture and fisheries, which are highly sensitive climate change and its extremes. Recent studies reported that the region is continuously experiencing climate extremes with substantial socioeconomic impacts (Rahman et al., 2019; Subash and Sikka, 2014; Yaduvanshi et al., 2019). The warming tendency of temperature may result in rising sea level and can pose potential threats to the coastal regions in the coming decades (Revadekar et al., 2013; Schleussner et al., 2016). It is believed that a slight increase in temperature may worsen the situation and can triggers climate extremes including heat waves and drought in the said region (Bhutiyani et al., 2007; Ratnam et al., 2016).

Despite the facts that we used the raw outputs of the CMIP5 models to project the future changes in temperature over SA at different warming levels above the pre-industrial levels, yet the estimated changes reported in this study are in line with the findings of the some regional studies, which have used downscaled outputs of the models. In this regard, we provided a comparative summary of the findings presented by such regional studies over the target region. Recently, Janes et al. (2019) used three downscaled runs of GCMs over SA and projected an average increase of 4.5°C in summer temperature over most parts during 2070–2099, with a maximum increase in the Himalayas, Pakistan and Eastern Afghanistan. Sanjay et al. (2017) employed downscaled runs of regional climate models over SA and estimated 5.4°C and 4.9°C warming in winter and summer temperature by the end of 21st century under RCP8.5 scenario. Ahsan et al. (2018) projected future T_{mean} over the Kabul River Basin using a MMEM of high-resolution statistically downscaled CMIP5 models. They reported an increase of 3.2°C and 5.8°C in annual and seasonal temperature across the basin under RCP4.5 and RCP8.5 scenarios by the mid-century, respectively. Mahmood and Jia (2017) conducted a study in the Indo-Pak territories of Jhelum River basin and projected a sharp increase in T_{min} and T_{max} from downscaled CMIP5 GCMs during 2041–2070 under RCP8.5 scenario relative to the present climate.

Similarly, Su et al. (2016) projected significant rise in annual T_{mean} by using the downscaled outputs of CMIP5 models over the Indus River Basin. They reported an increase of 1.21°C, 1.93°C, and 2.71°C under

RCP2.6, RCP4.5 and RCP8.5 scenarios by the end of the 21st century relative to the baseline period (1986-2005), respectively. Cuba et al. (2017) employed two downscaled GCMs over Tamil Nadu, India and predict that the T_{min} and T_{max} are likely to increase by 0.20 °C (0.45°C) and 0.17°C (0.42°C) under RCP4.5 (RCP8.5) scenario by the end of the 21st century, respectively. Ali et al. (2019) used the downscaled CMIP5 models and indicated that the T_{mean} is projected to increase by 0.8 °C, 1.5 °C, and 2.2 °C (1.2 °C, 2.5 °C and 4.5 °C) in the 2020s, 2050s and 2080s over different climatic regions of Pakistan under RCP4.5 (RCP8.5) scenario, respectively. Similarly, the downscaled runs of CMIP5 suggest that Pakistan is likely to experience a rise in T_{min} and summer days in the range of 1.3–1.9 °C and 6–20 days by the year of 2045 under both RCP4.5 and RCP8.5 scenarios (Sajjad and Ghaffar, 2019). According to (Ahmad et al. 2014; Ahmad et al. 2014), the downscaled models project a 1–1.5 °C and 1.5–2 °C rise in T_{mean} over different parts Pakistan in the near future (2007-2027) and the far future (2080-2099) periods relative to the baseline (1979-1998) period. In addition, several studies based on high-resolution downscaled models anticipated a sharp increase in temperature and its extremes over Pakistan during 21st century, with substantial impacts in the northwestern and southeastern parts of the country (Amin et al., 2018a, 2018b; Nasim et al., 2018; Saeed et al., 2017).

Recently, Khan et al. (2020a, 2020b) estimated future changes in seasonal and annual temperature over Bangladesh at 1.5 °C 2 °C, and 4 °C warming levels with high-resolution downscaled models and reported that the country is likely to experience a sharp rise in T_{min} and T_{max} in the range of 0.54–4.17 and 0.69–-4.55°C under RCP8.5 scenario by the end of 21st century with respect to the base (1986-2005) period. In another study, Alamgir et al. (2019) revealed a rise in T_{min} by 2.1–4.2 °C and 3.2–5.1 °C and T_{max} by 1.3–2.9 °C and 2.2–4.3 °C in different parts of Bangladesh under RCP4.5 and RCP8.5 scenarios during the period of 2070–2099 with respect to the present world, respectively. According to Hasan et al. (2018), the simulations of downscaled CMIP5 models anticipated an obvious increase in daytime and nighttime temperatures over Bangladesh with maximum intensity in the northeastern parts under RCP4.5 and RCP8.5 scenarios by the end of the 21st century. In another study, Rahman et al. (2012) employed a regional climate model over Bangladesh and projected a rise in T_{mean} in different months within the range of 0.5–2.1°C and 0.9–3.5°C for the year 2050 and 2060, respectively. It is worth-mentioned that the aforementioned studies have indicated a sharp increase in temperature over most parts of SA, with maximum intensity in the Himalayas, western India, eastern Pakistan, and eastern Afghanistan. Moreover, the studies based on downscaled approach have projected more warming in the high altitude regions of SA and have linked this warming tendency with elevation-dependent warming (Ali et al., 2019; Janes et al., 2019; Mahmood and Jia, 2017; Sanjay et al., 2017). It is should be noted that the range of temperature changes suggested by these studies is in agreement with our findings, which can enhance the credibility of the results presented here. Although, there are slight variations in the intensity of temperature reported by the above-mentioned; however, these variations could be associated with the use of different methods, type and number of models, and/or different temporal periods.

5. Conclusions

This study intends to evaluate the spatial and temporal capability of the 21 CMIP5 models in the simulation of historical temperature and rank these models consequently. Furthermore, this study aims to project the future changes in T_{min}, T_{max}, and T_{mean} over SA using MMEMs under global warming of 1.5 °C, 2 °C and 3 °C. The results show that the CSIRO–MK3–6–0, MIROC–ESM–CHEM, CNRM–CM5, CCSM4, and MRI–CGCM3 are found the optimal models with an accurate and consistent spatiotemporal simulation of T_{min}, T_{max} and T_{mean} over SA. The MMEMs of T_{min}, T_{max}, and T_{mean} reveal that the changes in temperature over SA are faster than that of global average changes under both emission scenarios, which reflects its degree of vulnerability to climate change. Corresponding to 1.5 °C, 2 °C, and 3 °C warming levels, the study region will witness a rise in T_{min}, T_{max}, and T_{mean} under RCP4.5 and RCP8.5 scenarios with respect to the pre–industrial levels. Moreover, the spatial analysis of T_{min}, T_{max}, and T_{mean} shows a dominating and a consistent warming pattern across SA with stronger intensity in the higher latitude than mid–low latitudes under three warming targets and two emission scenarios. It has been observed that the northwestern (eastern) parts of SA will experience a maximum (minimum) rise in warming of T_{min}, T_{max}, and T_{mean} under 1.5 °C, 2 °C, and 3 °C warming thresholds in both emission scenarios with respect to the pre–industrial levels. Furthermore, the central and southern parts of SA will witness a moderate increase in T_{min}, T_{max}, and T_{mean} during 1.5 °C, 2 °C, and 3 °C warming targets under RCP4.5 and RCP8.5 scenarios. Interestingly, the warming patterns of T_{min}, T_{max}, and T_{mean} in response to 1.5 °C, 2 °C, and 3 °C warming thresholds are higher under the RCP4.5 scenario than the RCP8.5 scenario relative to the pre–industrial levels. In addition, the results indicate that T_{min} increases at a faster rate than T_{max} and T_{mean} under all warming targets during both emission scenarios. The uneven patterns of T_{min}, T_{max}, and T_{mean}, will be escalated across the study region; therefore, more attention should be paid to regional differences in response to global warming of 1.5 °C, 2 °C, and 3 °C targets. This study further recommends to project changes in climate extremes over SA under different warming levels, which will be helpful in the adaptation and mitigation of climate change over the study region.

Author contributions

Conceptualization, Safi Ullah and Qinglong You: Methodology, Safi Ullah, Qinglong You, Yuqing Zhang: Software, Asher Samuel Bhatti, Waheed Ullah, Daniel Fiifi Tawia Hagan: Data curation, Gohar Ali, Waheed Ullah, Yunqing Zhang: Validation, Waheed Ullah, Daniel Fiifi Tawia Hagan, Yuqing Zhang: Writing- Original draft preparation. Safi Ullah: Visualization: Asif Ali, Shah Nawaz Khan: Supervision, Qinglong You: Reviewing and Editing, Qinglong You, Amjad Ali, Mushtaq Ahmad Jan: Funding, Qinglong You. All authors have read and agreed for submission of the manuscript.

Declaration of Competing Interest

The authors declare that they have no known competing financial interests or personal relationships that could have appeared to influence the work reported in this paper.

Acknowledgement

This study was supported by National Key R&D Program of China (2017YFA0603804) and National Natural Science Foundation of China (41771069). The authors acknowledge the World Climate Research Programme's (WCRP) Working Group on Coupled Modeling (WGCM), which is responsible for CMIP. The authors are also thankful to the climate modeling groups (listed in Table 1 of this paper) for producing and making available their CMIP5 model outputs. The authors are grateful to the developers' of CRU for providing gridded temperature datasets.

References

Aadhar, S., Mishra, V., 2019. A Substantial rise in the area and population affected by dryness in South Asia. Environ. Res. Lett. 1–19 Acceptd.
Aadhar, S., Mishra, V., 2020. Increased drought risk in South Asia under warming climate: Implications of uncertainty in potential evapotranspiration estimates. J. Hydrometeorol. 1–46 Accepted.
Abbas, F., Rehman, I., Adrees, M., Ibrahim, M., Saleem, F., Ali, S., Rizwan, M., Salik, M.R., 2018. Prevailing trends of climatic extremes across Indus-Delta of Sindh-Pakistan. Theor. Appl. Climatol. 131, 1101–1117.

ADB, W.B., 2010. Pakistan Floods 2010: Preliminary Damage and Needs Assessment. Asian Development Bank and World Bank, Islamabad, Pakistan.
Adnan, S., Ullah, K., Gao, S., 2015. Characterization of drought and its assessment over Sindh, Pakistan during 1951-2010. J. Meteorol. Res. 29, 837–857.
Ahmad, B., Rasul, G., Iqbal, W., Bukhari, S.A.A., 2014. Regional comparison between global circulation model GCM20 and regional climate model PRECIS. Pakisan J. Meteorol. 11, 39–51.
Ahmad, W., Fatima, A., Awan, U.K., Anwar, A., 2014. Analysis of long term meteorological trends in the middle and lower Indus Basin of Pakistan-A non-parametric statistical approach. Glob. Planet. Chang. 122, 282–291.
Ahmed, K., Shahid, S., Harun, S. Bin, Wang, X., 2016. Characterization of seasonal droughts in Balochistan Province, Pakistan. Stoch. Env. Res. Risk A. 30, 747–762.
Ahmed, K., Shahid, S., Nawaz, N., 2018. Impacts of climate variability and change on seasonal drought characteristics of Pakistan. Atmos. Res. 214, 364–374.
Ahmed, K., Sachindra, D.A., Shahid, S., Demirel, M.C., Chung, E.-S., 2019a. Selection of multi-model ensemble of general circulation models for the simulation of precipitation and maximum and minimum temperature based on spatial assessment metrics. Hydrol. Earth Syst. Sci. 23, 4803–4824.
Ahmed, K., Shahid, S., Sachindra, D.A., Nawaz, N., Chung, E., Engineering, C., Teknologi, U., Bahru, J., 2019b. Fidelity assessment of general circulation model simulated precipitation and temperature over Pakistan using a feature selection method. J. Hydrol. 573, 281–298.
Ahmed, K., Shahid, S., Wang, X., Nawaz, N., Khan, N., 2019c. Spatiotemporal changes in aridity of Pakistan during 1901–2016. Hydrol. Earth Syst. Sci. 23, 3081–3096.
Ahmed, K., Sachindra, D.A., Shahid, S., Iqbal, Z., Nawaz, N., 2020a. Multi-model ensemble predictions of precipitation and temperature using machine learning algorithms. Atmos. Res. 236, 1–14.
Ahmed, K., Shahid, S., Chung, E., Nawaz, N., Khan, N., Rasheed, B., 2020b. Divergence of Potential Evapotranspiration Trends over Pakistan During 1967 – 2016.
Ahsan, S., Bokhari, A., Ahmad, B., Ali, J., Ahmad, S., Mushtaq, H., Rasul, G., 2018. Future Climate Change Projections of the Kabul River Basin Using a Multi-model Ensemble of High-Resolution Statistically Downscaled Data. Earth Syst. Environ. 2, 477–497.
Alam, A., Ahmed, B., Sammonds, P., 2020. Flash flood susceptibility assessment using the parameters of drainage basin morphometry in SE Bangladesh. Quat. Int. https://doi.org/10.1016/j.quaint.2020.04.047. (Accepted).
Alamgir, M., Ahmed, K., Homsi, R., Dewan, A., Jun, J., Shahid, S., 2019. Downscaling and projection of spatiotemporal changes in temperature of Bangladesh. Earth Syst. Environ. 3, 381–398.
Ali, S., Eum, H. Il, Cho, J., Dan, L., Khan, F., Dairaku, K., Shrestha, M.L., Hwang, S., Nasim, W., Khan, I.A., Fahad, S., 2019. Assessment of climate extremes in future projections downscaled by multiple statistical downscaling methods over Pakistan. Atmos. Res. 222, 114–133.
Ali, G., Bao, Y., Ullah, W., Ullah, S., Guan, Q., Liu, X., Li, L., Lei, Y., Li, G., Ma, J., 2020. Spatiotemporal trends of aerosols over urban regions in Pakistan and their possible links to meteorological parameters. Atmosphere (Basel). 11, 1–28.
Almazroui, M., Saeed, S., Saeed, F., Islam, M.N., Ismail, M., 2020. Projections of precipitation and temperature over the South Asian Countries in CMIP6. Earth Syst. Environ. 4, 1–24.
Amin, A., Nasim, W., Fahad, S., Ali, S., Ahmad, S., Rasool, A., Saleem, N., Refat, S., Mubeen, M., Ahmad, N., Mustafa, G., Adnan, M., Noor, M., Basir, A., Saud, S., Habib, M., Paz, J.O., 2018a. Evaluation and analysis of temperature for historical (1996–2015) and projected (2030–2060) climates in Pakistan using SimCLIM climate model: Ensemble application. Atmos. Res. 213, 422–436.
Amin, A., Nasim, W., Mubeen, M., Sarwar, S., Urich, P., Ahmad, A., Wajid, A., Khaliq, T., Rasul, F., Hammad, H.M., Rehmani, M.I.A., Mubarak, H., Mirza, N., Wahid, A., Ahamd, S., Fahad, S., Ullah, A., Khan, M.N., Ameen, A., Amanullah Shahzad, B., Saud, S., Alharby, H., Ata-Ul-Karim, S.T., Adnan, M., Islam, F., Ali, Q.S., 2018b. Regional climate assessment of precipitation and temperature in Southern Punjab (Pakistan) using SimCLIM climate model for different temporal scales. Theor. Appl. Climatol. 131, 121–131.
Amirataee, B., Montaseri, M., Rezaie, H., 2018. Regional analysis and derivation of copula-based drought Severity-Area-Frequency curve in Lake Urmia basin, Iran. J. Environ. Manage. 206, 134–144.
Asmat, U., Athar, H., 2017. Run-based multi-model interannual variability assessment of precipitation and temperature over Pakistan using two IPCC AR4-based AOGCMs. Theor. Appl. Climatol. 127, 1–16.
Azad, A.K., Hossain, K.M., Nasreen, M., 2013. Flood-induced vulnerabilities and problems encountered by women in northern Bangladesh. Int. J. Disaster Risk Sci. 4, 190–199. https://doi.org/10.1007/s13753-013-0020-z.
Bhatti, A.S., Wang, G., Ullah, W., Ullah, S., Hagan, D.F.T., Nooni, I.K., Lou, D., Ullah, I., 2020. Trend in extreme precipitation indices based on long term in situ precipitation records over Pakistan. Water 12, 1–19.
Bhutiyani, M.R., Kale, V.S., Pawar, N.J., 2007. Long-term trends in maximum, minimum and mean annual air temperatures across the Northwestern Himalaya during the twentieth century. Clim. Chang. 85, 159–177.
Bocchiola, D., Diolaiuti, G., 2013. Recent (1980-2009) evidence of climate change in the upper Karakoram, Pakistan. Theor. Appl. Climatol. 113, 611–641.
Byers, E., Gidden, M., Leclere, D., Balkovic, J., Burek, P., Ebi, K., Greve, P., Grey, D., Havlik, P., Hillers, A., Johnson, N., Kahil, T., Krey, V., Langan, S., Nakicenovic, N., Novak, R., Obersteiner, M., Pachauri, S., Palazzo, A., Parkinson, S., Rao, N.D., Rogelj, J., Satoh, Y., Wada, Y., Willaarts, B., Riahi, K., 2018. Global exposure and vulnerability to multi-sector development and climate change hotspots Global exposure and vulnerability to multi-sector development and climate change hotspots. Environ. Res. Lett. 13, 1–14.
Chen, F., Chen, J., Huang, W., Chen, S., Huang, X., Jin, L., Jia, J., Zhang, X., An, C., Zhang, J., Zhao, Y., Yu, Z., Zhang, R., Liu, J., Zhou, A., Feng, S., 2019. Westerlies Asia and monsoonal Asia: Spatiotemporal differences in climate change and possible mechanisms on decadal to sub-orbital timescales. Earth-Sci. Rev. 192, 337–354.
Cheng, C.S., Auld, H., Li, Q., Li, G., 2012. Possible impacts of climate change on extreme weather events at local scale in south-central Canada. Clim. Chang. 112, 963–979.
Collier, M.A., Jeffrey, S.J., Rotstayn, L.D., Dravitzki, S.M., Moeseneder, C., Hamalainen, C., Syktus, J.I., Suppiah, R., Antony, J., El Zein, A., Atif, M., 2011. The CSIRO-Mk3.6.0 Atmosphere-Ocean GCM: participation in CMIP5 and data publication. In: 19th International Congress on Modelling and Simulation, Perth, Australia, pp. 2691–2697.
Colón-González, F.J., Harris, I., Osborn, T.J., Steiner São Bernardo, C., Peres, C.A., Hunter, P.R., Lake, I.R., 2018. Limiting global-mean temperature increase to 1.5–2 °C could reduce the incidence and spatial spread of dengue fever in Latin America. Proc. Natl. Acad. Sci. 115, 6243–6248.
Cuba, P., Jagannathan, R., Sathyamoorthy, N.K., Balasubramanian, R., Panneerselam, S., 2017. Dynamically downscaled CMIP5 model climate change projections for Tamil Nadu. J. Agrometeorol. 19, 32–37.
Das, L., Meher, J.K., 2019. Drivers of climate over the Western Himalayan region of India: A review. Earth-Sci. Rev. 198, 1–15.
Das, L., Dutta, M., Mezghani, A., Benestad, R.E., 2018. Use of observed temperature statistics in ranking CMIP5 model performance over the Western Himalayan Region of India. Int. J. Climatol. 38, 554–570.
Dash, S.K., Sharma, N., Pattnayak, K.C., Gao, X.J., Shi, Y., 2012. Temperature and precipitation changes in the north-east India and their future projections. Glob. Planet. Chang. 98–99, 31–44.
Dimri, A.P., Niyogi, D., Barros, A.P., Ridley, J., Mohanty, U.C., Yasunari, T., Sikka, D.R., 2015. Western disturbances: A review. Rev. Geophys. 53, 225–246.
Dimri, A.P., Kumar, D., Choudhary, A., Maharana, P., 2018a. Future changes over the Himalayas: Maximum and minimum temperature. Glob. Planet. Chang. 162, 212–234.
Dimri, A.P., Kumar, D., Choudhary, A., Maharana, P., 2018b. Future changes over the Himalayas : Mean temperature. Glob. Planet. Chang. 162, 235–251.
Donnelly, C., Greuell, W., Andersson, J., Gerten, D., Pisacane, G., Roudier, P., Ludwig, F., 2017. Impacts of climate change on European hydrology at 1.5, 2 and 3 degrees mean global warming above preindustrial level. Clim. Chang. 143, 13–26.
Dosio, A., Fischer, E.M., 2018. Will half a degree make a difference? Robust projections of Indices of mean and extreme climate in Europe under 1.5°C, 2°C, and 3°C global warming. Geophys. Res. Lett. 45, 935–944.
Dosio, A., Mentaschi, L., Fischer, E.M., Wyser, K., 2018. Extreme heat waves under 1.5 and 2 degree global warming. Environ. Res. Lett. 13, 1–10.
Filippi, L., Palazzi, E., von Hardenberg, J., Provenzale, A., 2014. Multidecadal variations in the relationship between the NAO and winter precipitation in the Hindu Kush–Karakoram. J. Clim. 27, 7890–7902.
Fischer, E.M., 2014. Autopsy of two mega-heatwaves. Nat. Geosci. 7, 332–333.
Fischer, E.M., Sedláček, J., Hawkins, E., Kutti, R., 2014. Models agree on forced response pattern of precipitation and temperature extremes. Geophys. Res. Lett. 41, 8554–8562.
Ford, J.D., Pearce, T., McDowell, G., Berrang-Ford, L., Sayles, J.S., Belfer, E., 2018. Vulnerability and its discontents: the past, present, and future of climate change vulnerability research. Clim. Chang. 151, 189–203.
Fowler, H.J., Archer, D.R., 2006. Conflicting signals of climatic change in the upper Indus Basin. J. Clim. 19, 4276–4293.
Galarneau, T.J., Hamill, T.M., Dole, R.M., Perlwitz, J., 2012. A multiscale analysis of the extreme weather events over Western Russia and Northern Pakistan during July 2010. Mon. Weather Rev. 140, 1639–1664.
Gu, H., Wang, G., Yu, Z., Mei, R., 2012. Assessing future climate changes and extreme indicators in east and south Asia using the RegCM4 regional climate model. Clim. Chang. 114, 301–317.
Guo, D., Yu, E., Wang, H., 2016. Will the tibetan plateau warming depend on elevation in the future? J. Geophys. Res. Atmos. 121, 3969–3978.
Guo, X., Huang, J., Luo, Y., Zhao, Z., Xu, Y., 2017. Projection of heat waves over China for eight different global warming targets using 12 CMIP5 models. Theor. Appl. Climatol. 128, 507–522.
Gupta, V., Jain, M.K., 2018. Investigation of multi-model spatiotemporal mesoscale drought projections over India under climate change scenario. J. Hydrol. 567, 489–509.
Gusain, A., Ghosh, S., Karmakar, S., 2020. Added value of CMIP6 over CMIP5 models in simulating Indian summer monsoon rainfall. Atmos. Res. 232, 1–8.
Hagan, D.F.T., Wang, G.J., Parinussa, R.M., Shi, X., 2019. Inter-comparing and improving land surface temperature estimates from passive microwaves over the Jiangsu province of the People's Republic of China. Int. J. Remote Sens. 40, 5563–5584.
Haq, Z.-U., Tariq, S., Ali, M., 2017. Spatiotemporal patterns of correlation between atmospheric nitrogen dioxide and aerosols over South Asia. Meteorog. Atmos. Phys. 129, 507–527.
Harris, I., Jones, P.D., Osborn, T.J., Lister, D.H., 2014. Updated high-resolution grids of monthly climatic observations-the CRU TS3.10 Dataset. Int. J. Climatol. 34, 623–642.
Hasan, M.A., Islam, A.K.M.S., Shafqat, A., 2018. Climate projections and extremes in dynamically downscaled CMIP5 model outputs over the Bengal delta : a quartile based bias-correction approach with new gridded data. Clim. Dyn. 51, 2169–2190.
Hunt, K.M.R., Turner, A.G., Shaffrey, L.C., 2018. The evolution, seasonality and impacts of western disturbances. Q. J. R. Meteorol. Soc. 144, 278–290.
Im, E.S., Pal, J.S., Eltahir, E.A.B., 2017. Deadly heat waves projected in the densely populated agricultural regions of South Asia. Sci. Adv. 3, 1–8.
IPCC, 2018. Global Warming of 1.5°C. Geneva, Switzerland, Intergovernamental Panel on Climate Change, Geneva, Switzerland.
Jacob, D., Kotova, L., Teichmann, C., Sobolowski, S.P., Vautard, R., Donnelly, C., Koutroulis, A.G., Grillakis, M.G., Tsanis, I.K., Damm, A., Sakalli, A., Van Vliet,

M.T.H., Centre, B., Ipsl, L., Uvsq, C.E.A.C., 2018. Earth's future climate impacts in Europe under +1.5°C global warming earth's future. Earth's Futur. 6, 264–285.
Janes, T., Mcgrath, F., Macadam, I., Jones, R., 2019. Environment High-resolution climate projections for South Asia to inform climate impacts and adaptation studies in the Ganges-Brahmaputra-Meghna and Mahanadi deltas. Sci. Total Environ. 650, 1499–1520.
Jhajharia, D., Shrivastava, S.K., Sarkar, D., Sarkar, S., 2009. Temporal characteristics of pan evaporation trends under the humid conditions of northeast India. Agric. For. Meteorol. 149, 763–770.
Jhajharia, D., Dinpashoh, Y., Kahya, E., Singh, V.P., Fakheri-Fard, A., 2012. Trends in reference evapotranspiration in the humid region of northeast India. Hydrol. Process. 26, 421–435.
Jiang, Z., Li, W., Xu, J., Li, L., 2015. Extreme precipitation indices over China in CMIP5 models. Part I: Model evaluation. J. Clim. 28, 8603–8619.
Jones, B., Neill, B.C.O., 2016. Spatially explicit global population scenarios consistent with the Shared Socioeconomic Pathways Spatially explicit global population scenarios consistent with the Shared Socioeconomic Pathways. Environ. Res. Lett. 11, 1–10.
Joshi, S., Kar, S.C., 2018. Mechanism of ENSO influence on the South Asian monsoon rainfall in global model simulations. Theor. Appl. Climatol. 131, 1449–1464.
Khan, N., Ahmed, M., Wahab, M., Zafar, M.U., Buckley, B.M., Palmer, J., Rao, M.P., 2015. Karakorum temperature out of phase with hemispheric trends for the past five centuries. Clim. Dyn. 46, 1943–1952.
Khan, N., Shahid, S., Ismail, T. Bin, Wang, X.-J., 2018a. Spatial distribution of unidirectional trends in temperature and temperature extremes in Pakistan. Theor. Appl. Climatol. 18, 1–15.
Khan, N., Shahid, S., Ismail, T., Ahmed, K., Nawaz, N., 2018b. Trends in heat wave related indices in Pakistan. Stoch. Env. Res. Risk A. 2, 1–16.
Khan, N., Shahid, S., Juneng, L., Ahmed, K., Ismail, T., Nawaz, N., 2019. Prediction of heat waves in Pakistan using quantile regression forests. Atmos. Res. 221, 1–11.
Khan, M.J.U., Islam, A.K.M.S., Bala, S.K., Islam, G.M.T., 2020a. Changes in climate extremes over Bangladesh at 1.5 °C, 2 °C, and 4 °C of global warming with high-resolution regional climate modeling. Theor. Appl. Climatol. 140, 1451–1466.
Khan, N., Shahid, S., Ahmed, K., Wang, X., Ali, R., Ismail, T., Nawaz, N., 2020b. Selection of GCMs for the projection of spatial distribution of heat waves in Pakistan. Atmos. Res. 233, 1–14.
Kharin, V.V., Zwiers, F.W., Zhang, X., Wehner, M., 2013. Changes in temperature and precipitation extremes in the CMIP5 ensemble. Clim. Chang. 119, 345–357.
King, A.D., Karoly, D.J., Henley, B.J., 2017. Australian climate extremes at 1.5 °C and 2 °C of global warming. Nat. Clim. Chang. 7, 412–416.
Kraaijenbrink, P.D.A., Bierkens, M.F.P., Lutz, A.F., Immerzeel, W.W., 2017. Impact of a global temperature rise of 1.5 degrees Celsius on Asia's glaciers. Nature 549, 257–260.
Kripalani, R.H., Oh, J.H., Kulkarni, A., Sabade, S.S., Chaudhari, H.S., 2007. South Asian summer monsoon precipitation variability: Coupled climate model simulations and projections under IPCC AR4. Theor. Appl. Climatol. 90, 133–159.
Kumar, P., Rupa Kumar, K., Rajeevan, M., Sahai, A.K., 2007. On the recent strengthening of the relationship between ENSO and northeast monsoon rainfall over South Asia. Clim. Dyn. 28, 649–660.
Latif, M., Syed, F.S., Hannachi, A., 2017. Rainfall trends in the South Asian summer monsoon and its related large-scale dynamics with focus over Pakistan. Clim. Dyn. 48, 3565–3581.
Latif, M., Hannachi, A., Syed, F.S., 2018. Analysis of rainfall trends over Indo-Pakistan summer monsoon and related dynamics based on CMIP5 climate model simulations. Int. J. Climatol. 38, 577–595.
Lee, S.M., Min, S.K., 2018. Heat stress changes over East Asia under 1.5° and 2.0°C global warming targets. J. Clim. 31, 2819–2831.
Lehner, F., Coats, S., Stocker, T.F., Pendergrass, A.G., Sanderson, B.M., Raible, C.C., Smerdon, J.E., 2017. Projected drought risk in 1.5°C and 2°C warmer climates. Geophys. Res. Lett. 44, 7419–7428.
Li, R., Lv, S., Han, B., Gao, Y., Meng, X., 2017. Projections of South Asian summer monsoon precipitation based on 12 CMIP5 models. Int. J. Climatol. 37, 94–108.
Li, D., Zhou, T., Zou, L., Zhang, W., Zhang, L., 2018. Extreme high-temperature events over East Asia in 1.5°C and 2°C warmer futures: analysis of NCAR CESM low-warming experiments. Geophys. Res. Lett. 45, 1541–1550.
Liu, W., Sun, F., Lim, W.H., Zhang, J., Wang, H., Shiogama, H., Zhang, Y., 2018. Global drought and severe drought-affected populations in 1.5 and 2 °C warmer worlds. Earth Syst. Dyn. 9, 267–283.
Mahmood, R., Jia, S., 2016. Assessment of impacts of climate change on the water resources of the transboundary Jhelum River Basin of Pakistan and India. Water 8, 246–264.
Mahmood, R., Jia, S., 2017. An extended linear scaling method for downscaling temperature and its implication in the Jhelum River basin, Pakistan, and India, using CMIP5 GCMs. Theor. Appl. Climatol. 130, 725–734.
Mahmood, R., Babel, M.S., Jia, S., 2015. Assessment of temporal and spatial changes of future climate in the Jhelum river basin, Pakistan and India. Weather Clim. Extrem. 10, 40–55.
Mazdiyasni, O., AghaKouchak, A., Davis, S.J., Madadgar, S., Mehran, A., Ragno, E., Sadegh, M., Sengupta, A., Ghosh, S., Dhanya, C.T., Niknejad, M., 2017. Increasing probability of mortality during Indian heat waves. Sci. Adv. 3, 1–6.
Medina, S., Houze, R.A., Kumar, A., Niyogi, D., 2010. Summer monsoon convection in the Himalayan region: Terrain and land cover effects. Q. J. R. Meteorol. Soc. 136, 593–616.
Miao, C., Duan, Q., Sun, Q., Li, J., 2013. Evaluation and application of Bayesian multimodel estimation in temperature simulations. Prog. Phys. Geogr. 37, 727–744.
Miao, C., Duan, Q., Sun, Q., Huang, Y., Kong, D., Yang, T., Ye, A., Di, Z., Gong, W., 2014. Assessment of CMIP5 climate models and projected temperature changes over Northern Eurasia. Environ. Res. Lett. 9, 1–12.
Mishra, V., Mukherjee, S., Kumar, R., Stone, D.A., 2017. Heat wave exposure in India in current, 1.5°C, and 2°C worlds. Environ. Res. Lett. 12, 1–9.
Moss, R.H., Edmonds, J.A., Hibbard, K.A., Manning, M.R., Rose, S.K., van Vuuren, D.P., Carter, T.R., Emori, S., Kainuma, M., Kram, T., Meehl, G.A., Mitchell, J.F.B., Nakicenovic, N., Riahi, K., Smith, S.J., Stouffer, R.J., Thomson, A.M., Weyant, J.P., Wilbanks, T.J., 2010. The next generation of scenarios for climate change research and assessment. Nature 463, 747.
Nangombe, S., Zhou, T., Zhang, W., Wu, B., Hu, S., Zou, L., Li, D., 2018. Record-breaking climate extremes in Africa under stabilized 1.5°C and 2°C global warming scenarios. Nat. Clim. Chang. 8, 375–380.
Nasim, W., Amin, A., Fahad, S., Awais, M., Khan, N., Mubeen, M., Wahid, A., Turan, V., Rehman, M.H., Ihsan, M.Z., Ahmad, S., Hussain, S., Mian, I.A., Khan, B., Jamal, Y., 2018. Future risk assessment by estimating historical heat wave trends with projected heat accumulation using SimCLIM climate model in Pakistan. Atmos. Res. 205, 118–133.
Naveendrakumar, G., Vithanage, M., Kwon, H.-H., Chandrasekara, S.S.K., Iqbal, M.C.M., Pathmarajah, S., Fernando, W.C.D.K., Obeysekera, J., 2019. South Asian perspective on temperature and rainfall extremes: A review. Atmos. Res. 225, 110–120.
New, M., Lister, D., Hulme, M., Makin, I., 2002. A high-resolution data set of surface climate over global land areas. Clim. Res. 21, 1–25.
Noor, M., Ismail, T. Bin, Shahid, S., Ahmed, K., Chung, E.-S., Nawaz, N., 2019. Selection of CMIP5 multi-model ensemble for the projection of spatial and temporal variability of rainfall in peninsular Malaysia. Theor. Appl. Climatol. 138, 999–1012.
Panda, D.K., AghaKouchak, A., Ambast, S.K., 2017. Increasing heat waves and warm spells in India, observed from a multiaspect framework. J. Geophys. Res. Atmos. 122, 3837–3858.
Panday, P.K., Thibeault, J., Frey, K.E., 2014. Changing temperature and precipitation extremes in the Hindu Kush-Himalayan region: an analysis of CMIP3 and CMIP5 simulations and projections. Int. J. Climatol. 35, 3058–3077.
Pathak, A., Ghosh, S., Alejandro Martinez, J., Dominguez, F., Kumar, P., 2017a. Role of oceanic and land moisture sources and transport in the seasonal and interannual variability of summer monsoon in India. J. Clim. 30, 1839–1859.
Pathak, A., Ghosh, S., Kumar, P., Murtugudde, R., 2017b. Role of oceanic and terrestrial atmospheric moisture sources in intraseasonal variability of Indian summer monsoon rainfall. Sci. Rep. 7, 1–11.
Pepin, N., Bradley, R.S., Diaz, H.F., Baraer, M., Caceres, E.B., Forsythe, N., Fowler, H., Greenwood, G., Hashmi, M.Z., Liu, X.D., Miller, J.R., Ning, L., Ohmura, A., Palazzi, E., Rangwala, I., Schöner, W., Severskiy, I., Shahgedanova, M., Wang, M.B., Williamson, S.N., Yang, D.Q., 2015. Elevation-dependent warming in mountain regions of the world. Nat. Clim. Chang. 5, 424–430.
Pervez, M.S., Henebry, G.M., 2015. Assessing the impacts of climate and land use and land cover change on the freshwater availability in the Brahmaputra River basin. J. Hydrol. Reg. Stud. 3, 285–311.
Rahman, M.S., Islam, A.R.M.T., 2019. Are precipitation concentration and intensity changing in Bangladesh overtimes? Analysis of the possible causes of changes in precipitation systems. Sci. Total Environ. 690, 370–387.
Rahman, A. Ur, Khan, A.N., 2011. Analysis of flood causes and associated socio-economic damages in the Hindukush region. Nat. Hazards 59, 1239–1260.
Rahman, M.M., Islam, M.N., Ahmed, A.U., Georgi, F., 2012. Rainfall and temperature scenarios for Bangladesh for the middle of 21st century using RegCM. J. Earth Syst. Sci. 121, 287–295.
Rahman, M., Islam, M., Bräuning, A., 2019. Species-specific growth resilience to drought in a mixed semi-deciduous tropical moist forest in South Asia. For. Ecol. Manag. 433, 487–496. https://doi.org/10.1016/j.foreco.2018.11.034.
Rajbhandari, R., Shrestha, A.B., Kulkarni, A., Patwardhan, S.K., Bajracharya, S.R., 2015. Projected changes in climate over the Indus river basin using a high resolution regional climate model (PRECIS). Clim. Dyn. 44, 339–357.
Ramachandran, S., Kedia, S., 2013. Aerosol optical properties over South Asia from ground-based observations and remote sensing: a review. Climate 1, 84–119.
Ramachandran, S., Kedia, S., Srivastava, R., 2012. Aerosol optical depth trends over different regions of India. Atmos. Environ. 49, 338–347.
Rangwala, I., Miller, J.R., 2012. Climate change in mountains: A review of elevation-dependent warming and its possible causes. Clim. Chang. 114, 527–547.
Rasmussen, K.L., Hill, A.J., Toma, V.E., Zuluaga, M.D., Webster, P.J., Houze, R.A., 2015. Multiscale analysis of three consecutive years of anomalous flooding in Pakistan. Q. J. R. Meteorol. Soc. 141, 1259–1276.
Ratnam, J.V., Behera, S.K., Ratna, S.B., Rajeevan, M., Yamagata, T., 2016. Anatomy of Indian heatwaves. Sci. Rep. 6, 1–11.
Ravi Kumar, K., Valsala, V., Tiwari, Y.K., Revadekar, J.V., Pillai, P., Chakraborty, S., Murtugudde, R., 2016. Intra-seasonal variability of atmospheric CO2 concentrations over India during summer monsoons. Atmos. Environ. 142, 229–237.
Rehman, N., Adnan, M., Ali, S., 2018. Assessment of CMIP5 climate models over south Asia and climate change projections over Pakistan under representative concentration pathways. Int. J. Glob. Warm. 16, 381–415.
Ren, Y.Y., Ren, G.Y., Sun, X.B., Shrestha, A.B., You, Q.L., Zhan, Y.J., Rajbhandari, R., Zhang, P.F., Wen, K.M., 2017. Observed changes in surface air temperature and precipitation in the Hindu Kush Himalayan region over the last 100-plus years. Adv. Clim. Chang. Res. 8, 148–156.
Revadekar, J.V., Hameed, S., Collins, D., Manton, M., Sheikh, M., Borgaonkar, H.P., Kothawale, D.R., Adnan, M., Ahmed, A.U., Ashraf, J., Baidya, S., Islam, N., Jayasinghearachchi, D., Manzoor, N., Premalal, K.H.M.S., Shreshta, M.L., 2013. Impact of altitude and latitude on changes in temperature extremes over South Asia during 1971-2000. Int. J. Climatol. 33, 199–209.
Roy, S. Sen, Mahmood, R., Niyogi, D., Lei, M., Foster, S.A., Hubbard, K.G., Douglas, E.,

Pielke, R., 2007. Impacts of the agricultural Green Revolution-induced land use changes on air temperatures in India. J. Geophys. Res. Atmos. 112, 1–13.
Sa'adi, Z., Shiru, M.S., Shahid, S., Ismail, T., 2020. Selection of general circulation models for the projections of spatio-temporal changes in temperature of Borneo Island based on CMIP5. Theor. Appl. Climatol. 139, 351–371.
Saeed, F., Almazroui, M., Islam, N., Khan, M.S., 2017. Intensification of future heat waves in Pakistan: a study using CORDEX regional climate models ensemble. Nat. Hazards 87, 1635–1647.
Sajjad, H., Ghaffar, A., 2019. Observed, simulated and projected extreme climate indices over Pakistan in changing climate. Theor. Appl. Climatol. 137, 255–281.
Salman, S.A., Shahid, S., Ismail, T., Ahmed, K., Wang, X., 2018. Selection of climate models for projection of spatiotemporal changes in temperature of Iraq with uncertainties. Atmos. Res. 213, 509–522.
Sanjay, J., Krishnan, R., Shrestha, A.B., Rajbhandari, R., Ren, G., 2017. Downscaled climate change projections for the Hindu Kush Himalayan region using CORDEX South Asia regional climate models. Adv. Clim. Chang. Res. 8, 185–198.
Schleussner, C.F., Lissner, T.K., Fischer, E.M., Wohland, J., Perrette, M., Golly, A., Rogelj, J., Childers, K., Schewe, J., Frieler, K., Mengel, M., Hare, W., Schaeffer, M., 2016. Differential climate impacts for policy-relevant limits to global warming: The case of 1.5°C and 2°C. Earth Syst. Dyn. 7, 327–351.
Seong, M.G., Suh, M.S., Kim, C., 2017. Intercomparison of prediction skills of ensemble methods using monthly mean temperature simulated by CMIP5 models. Asia-Pac. J. Atmos. Sci. 53, 339–351.
Shafiq, M., Kakar, M.A., 2007. Effects of drought on livestock sector in Balochistan Province of Pakistan. Int. J. Agric. Biol. 9, 657–665.
Shahid, S., Wang, X.J., Harun, S. Bin, Shamsudin, S.B., Ismail, T., Minhans, A., 2016. Climate variability and changes in the major cities of Bangladesh: observations, possible impacts and adaptation. Reg. Environ. Chang. 16, 459–471.
Sharma, C.S., Panda, S.N., Pradhan, R.P., Singh, A., Kawamura, A., 2016. Precipitation and temperature changes in eastern India by multiple trend detection methods. Atmos. Res. 180, 211–225.
Sheikh, M.M., Manzoor, N., Ashraf, J., Adnan, M., Collins, D., Hameed, S., Manton, M.J., Ahmed, A.U., Baidya, S.K., Borgaonkar, H.P., Islam, N., Jayasinghearachchi, D., Kothawale, D.R., Premalal, K.H.M.S., Revadekar, J.V., Shrestha, M.L., 2015. Trends in extreme daily rainfall and temperature indices over South Asia. Int. J. Climatol. 35, 1625–1637.
Singh, G.R., Jain, M.K., Gupta, V., 2019. Spatiotemporal assessment of drought hazard, vulnerability and risk in the Krishna River basin, India. Nat. Hazards 99, 611–635.
Su, B., Huang, J., Gemmer, M., Jian, D., Tao, H., Jiang, T., Zhao, C., 2016. Statistical downscaling of CMIP5 multi-model ensemble for projected changes of climate in the Indus River Basin. Atmos. Res. 178–179, 138–149.
Subash, N., Sikka, A.K., 2014. Trend analysis of rainfall and temperature and its relationship over India. Theor. Appl. Climatol. 117, 449–462.
Sun, Q., Miao, C., Duan, Q., Kong, D., Ye, A., Di, Z., Gong, W., 2014. Would the "real" observed dataset stand up? A critical examination of eight observed gridded climate datasets for China. Environ. Res. Lett. 9, 1–15.
Sun, X.B., Ren, G.Y., Shrestha, A.B., Ren, Y.Y., You, Q.L., Zhan, Y.J., Xu, Y., Rajbhandari, R., 2017. Changes in extreme temperature events over the Hindu Kush Himalaya during 1961–2015. Adv. Clim. Chang. Res. 8, 157–165.
Sun, Q., Miao, C., Duan, Q., Ashouri, H., Sorooshian, S., Hsu, K.L., 2018. A review of global precipitation data sets: data sources, estimation, and intercomparisons. Rev. Geophys. 56, 79–107.
Sylla, M.B., Faye, A., Giorgi, F., Diedhiou, A., Kunstmann, H., 2018. Projected heat stress under 1.5 °C and 2 °C global warming scenarios creates unprecedented discomfort for humans in West Africa. Earth's Futur. 6, 1029–1044.
Taylor, K.E., 2001. Summarizing multiple aspects of model performance in a single diagram. J. Geophys. Res. Atmos. 106, 7183–7192.
Taylor, K.E., Stouffer, R.J., Meehl, G.A., 2012. An overview of CMIP5 and the experiment design. Bull. Am. Meteorol. Soc. 93, 485–498.
Trenberth, K.E., Dai, A., Van Der Schrier, G., Jones, P.D., Barichivich, J., Briffa, K.R., Sheffield, J., 2014. Global warming and changes in drought. Nat. Clim. Chang. 4, 17–22.
Ullah, S., You, Q., Ullah, W., Ali, A., 2018a. Observed changes in precipitation in China-Pakistan economic corridor during 1980–2016. Atmos. Res. 210, 1–14.
Ullah, S., You, Q., Ullah, W., Ali, A., Xie, W., Xie, X., 2018b. Observed changes in temperature extremes over China-Pakistan economic corridor during 1980-2016. Int. J. Climatol. 39, 1457–1475.
Ullah, W., Wang, G., Ali, G., Tawia Hagan, D., Bhatti, A., Lou, D., 2019. Comparing multiple precipitation products against in-situ observations over different climate regions of Pakistan. Remote Sens. 11, 628.
Ullah, S., You, Q., Ali, A., Ullah, W., Jan, M.A., Zhang, Y., Xie, W., Xie, X., 2019a. Observed changes in maximum and minimum temperatures over China- Pakistan economic corridor during 1980–2016. Atmos. Res. 216, 37–51.
Ullah, S., You, Q., Ullah, W., Hagan, F.D.T., Ali, A., Ali, G., Zhang, Y., Jan, M.A., Bhatti, A.S., Xie, W., 2019b. Daytime and nighttime heat wave characteristics based on multiple indices over the China–Pakistan economic corridor. Clim. Dyn. 53, 6329–6349.
UNFCCC, 2015. Adoption of the Paris Agreement. Paris, France.
Wang, G., Hagan, D.F.T., Lou, D., Chen, T., 2016. Evaluation of soil moisture derived from FY3B microwave brightness temperature over the Tibetan Plateau. Remote Sens. Lett. 7, 817–826.
Wang, P.X., Wang, B., Cheng, H., Fasullo, J., Guo, Z.T., Kiefer, T., Liu, Z.Y., 2017a. The global monsoon across time scales: Mechanisms and outstanding issues. Earth-Sci. Rev. 174, 84–121.
Wang, X., Jiang, D., Lang, X., 2017b. Future extreme climate changes linked to global warming intensity. Sci. Bull. 62, 1673–1680.
Wang, G., Pan, J., Shen, C., Li, S., Lu, J., Lou, D., Hagan, D.F.T., 2018. Evaluation of evapotranspiration estimates in the Yellow River Basin against the water balance method. Water 10, 1–18.
Wehner, M., Stone, D., Krishnan, H., Achutarao, K., Castillo, F., 2016. The deadly combination of heat and humidity in India and Pakistan in summer 2015. Bull. Am. Meteorol. Soc. 97, S81–S86.
Wu, S., Liu, L., Liu, Y., Gao, J., Dai, E., Feng, A., Wang, W., 2019. The Belt and Road: Geographical pattern and regional risks. J. Geogr. Sci. 29, 483–495.
Wu, F., You, Q., Zhang, Z., Zhang, L., 2020. Changes and uncertainties of surface mean temperature over China under global warming of 1.5 ° C and 2 ° C. Int. J. Climatol. 40, 1–18.
Xie, H., Ringler, C., Zhu, T., Waqas, A., 2013. Droughts in Pakistan: A spatiotemporal variability analysis using the Standardized Precipitation Index. Water Int. 38, 620–631.
Xu, Y., Zhou, B.T., Wu, Jie, Han, Z.Y., Zhang, Y.X., Wu, Jia, 2017. Asian climate change under 1.5–4 °C warming targets. Adv. Clim. Chang. Res. 8, 99–107.
Xu, Y., Wu, X., Kumar, R., Barth, M., Diao, C., Gao, M., Lin, L., Jones, B., Meehl, G.A., 2020. Substantial increase in the joint occurrence and human exposure of heatwave and high-PM hazards Over South Asia in the Mid-21st Century. AGU Adv. 1, 1–19.
Yadav, S.S., Lal, R., 2018. Vulnerability of women to climate change in arid and semi-arid regions: The case of India and South Asia. J. Arid Environ. 149, 4–17.
Yaduvanshi, A., Zaroug, M., Bendapudi, R., New, M., 2019. Impacts of 1.5 °C and 2 °C global warming on regional rainfall and temperature change across India. Environ. Res. Lett. 1, 1–14.
You, Q., Ren, G.Y., Zhang, Y.Q., Ren, Y.Y., Sun, X.B., Zhan, Y.J., Shrestha, A.B., Krishnan, R., 2017a. An overview of studies of observed climate change in the Hindu Kush Himalayan (HKH) region. Adv. Clim. Chang. Res. 8, 141–147.
You, Q., Wang, D., Jiang, Z., Kang, S., 2017b. Diurnal temperature range in CMIP5 models and observations in the Tibetan Plateau. Q. J. R. Meteorol. Soc. 143, 1978–1989.
You, Q., Jiang, Z., Wang, D., Pepin, N., Kang, S., 2018. Simulation of temperature extremes in the Tibetan Plateau from CMIP5 models and comparison with gridded observations. Clim. Dyn. 51, 355–369.
You, Q., Zhang, Y., Xie, X., Wu, F., 2019. Robust elevation dependency warming over the Tibetan Plateau under global warming of 1.5°C and 2°C. Clim. Dyn. 53, 2047–2060.
You, Q., Wu, F., Shen, L., Pepin, N., Jiang, Z., Kang, S., 2020. Tibetan Plateau amplification of climate extremes under global warming of 1.5°C, 2°C and 3°C. Glob. Planet. Chang. 192, 1–10 (Accepted, 103261).
Zhang, Y., You, Q., Chen, C., Ge, J., Adnan, M., 2017. Evaluation of downscaled CMIP5 Coupled with VIC model for flash drought simulation in a humid subtropical basin, China. J. Clim. 31, 1075–1090.
Zhang, Y., You, Q., Mao, G., Chen, C., Ye, Z., 2018. Short-term concurrent drought and heatwave frequency with 1.5 and 2.0 °C global warming in humid subtropical basins: a case study in the Gan River Basin, China. Clim. Dyn. 52, 4621–4641.
Zheng, H., Chiew, F.H.S., Charles, S., Podger, G., 2018. Regional Studies Future climate and runoff projections across South Asia from CMIP5 global climate models and hydrological modelling. J. Hydrol. 18, 92–109.
Zhou, J., Jiang, T., Wang, Y., Su, B., Tao, H., Qin, J., Zhai, J., 2020. Spatiotemporal variations of aridity index over the Belt and Road region under the 1.5°C and 2.0°C warming scenarios. J. Geogr. Sci. 30, 37–52.